

Tunable Cooperative Motion, Rigidity, and Glassy Dynamics in Knotted Ring Polymer Melts

Yue-Tong Dong,^{†,‡} Jack F. Douglas,^{¶,§} and Wen-Sheng Xu^{*,†,‡}

[†]*State Key Laboratory of Polymer Science and Technology, Changchun Institute of Applied
Chemistry, Chinese Academy of Sciences, Changchun 130022, P. R. China*

[‡]*School of Applied Chemistry and Engineering, University of Science and Technology of
China, Hefei 230026, P. R. China*

[¶]*Materials Science and Engineering Division, National Institute of Standards and
Technology, Gaithersburg, Maryland 20899, United States*

[§]*NIST Fellow (emeritus).*

E-mail: wsxu@ciac.ac.cn

Abstract

We present a molecular dynamics study of the influence of knot complexity and molecular mass on glass formation upon cooling in knotted ring polymer melts. We find that cooperative motion, rigidity, and glassy dynamics can be tuned over a wide range by knots. By leveraging these knotting constraints, we assess the validity of prevalent models of glass formation, including the string model based on cooperative particle motion, the localization model emphasizing fluctuations in local particle mobility, and the shoving model derived from emergent elastic properties in relation to material stiffness. In line with our previous findings on polymeric and other glass-forming liquids, we demonstrate that all these models of glass formation provide a quantitative description of segmental relaxation as a function of knot complexity, molecular mass, and temperature, despite their apparently distinct conceptual foundations. Our study thus provides additional evidence for an underlying unity among various theoretical frameworks and for the presence of quantitative relations between the characteristic properties emphasized by these models. Furthermore, we discuss dynamic and elastic heterogeneities in relation to fragility and stiffness variations of knotted ring polymer melts, with a focus on how these trends relate to other glass-forming liquids where fragility is tuned over a large range.

1 Introduction

Glass-forming materials exhibit a dramatic slowdown in their dynamics upon cooling toward the glass transition temperature (T_g), despite the absence of significant changes in their overall static structure.¹⁻⁶ This complex phenomenon has motivated the development of a number of theoretical approaches based on distinct physical perspectives, such as local density-based free volume models,^{7,8} the Adam-Gibbs (AG) theory,⁹ the mode-coupling theory,¹⁰⁻¹² the random first-order transition theory,¹³ the string model,^{14,15} the localization model,^{16,17} the shoving model,¹⁸⁻²⁰ and a continually growing number of other approaches. These diverse models have yielded valuable insights into specific aspects of glass formation and stimulated extensive experimental and computational efforts to test their assumptions and predictions,¹⁻⁶ although a universally accepted theory of glass formation has not been established.

While the growing number of proposed models might be viewed as representing a disappointing lack of consensus on the nature of glass formation, their independent success in describing the dynamics of glass-forming materials suggests to us a possible unity underlying these models. Indeed, there has been progress made in this direction recently. Betancourt et al.²¹ presented evidence from simulations of polymeric glass-forming liquids in the bulk, thin supported films, and polymer nanocomposites that relaxation can be described reasonably well for all of the systems by different models based on cooperative motion, emergent elasticity, and dynamical free volume. Following this line of research, our recent works demonstrated that some of the existing models provide equally valid descriptions of glass formation in polymer melts having variable chain length and chain rigidity²² as well as in the canonical Kob-Andersen model system over a wide range of densities and pressures.²³ Moreover, the generalized entropy theory (GET) of polymer glass formation,²⁴⁻²⁷ which combines the lattice cluster theory^{28,29} for polymer thermodynamics and the AG relation⁹ relating the configurational entropy to the structural relaxation time, predicts close interrelations between the configurational entropy, configurational enthalpy, and configurational

internal energy,³⁰ bringing together these disparate thermodynamic viewpoints of glass formation.^{31–33} The reader is referred to a recent review for the detailed discussion of a unified thermodynamic perspective on glass formation.²⁶

In the present work, we extend our previous efforts in unifying various models of glass formation to a family of knotted ring polymer melts. Knots have been found in various polymeric systems, such as Deoxyribonucleic acid (DNA),^{34–36} proteins,^{37–39} and synthetic polymers.^{40–42} It has been widely appreciated that the physical properties of polymeric materials can significantly be impacted by knots, such as the tensile strength,⁴³ the relaxation rate of compressed polymers,⁴⁴ the diffusion of polymers in nanotubes,^{45,46} the dynamics and functionality of DNA and proteins,^{47–49} etc. Knotted ring polymers also serve as an ideal system for testing theoretical models of glass formation, since knotting can lead to large alterations in the characteristic properties of glass formation, such as collective motion and material stiffness. In our recent work based on extensive simulation results,⁵⁰ we examined the influence of knot complexity (quantified by the minimum crossing number m_c) and molecular mass on basic thermodynamic and segmental dynamic properties in knotted ring polymer melts, and inspired by the GET predictions,^{24,25} we rationalized the trends in T_g and fragility in terms of molecular packing frustration, where fragility is a property that characterizes the strength of the T dependence of the dynamics near T_g . Hence, leveraging these knotting constraints offers a promising avenue to illuminate longstanding theoretical questions concerning glass formation. As a particular advantage of studying glass-forming knotted ring polymers, and also star polymers,⁵¹ the characteristics of glass formation such as T_g and fragility can be varied over a large range without changing the monomer structure or molecular mass. Moreover, one can avoid phase separation and crystallization tendencies in popular glass-forming multi-component fluid mixtures, such as the Kob-Andersen model system.^{52,53} From a broader perspective, a deep understanding of how knotting influences glass formation provides important guidance for designing advanced polymeric materials with desired properties^{54–56} and holds direct relevance to understanding the physical properties

and biological functions of topologically complex biomacromolecules.^{57–59}

After a brief overview of relaxation in knotted ring polymer melts having variable knot complexity and molecular mass, we assess the validity of several models of glass formation. Specifically, we consider the string model,^{14,15} a variant of the entropy theory of glass formation emphasizing cooperative particle motion, the localization model emphasizing fluctuations in local particle mobility,^{16,17} and the shoving model derived from a focus on the emergent elastics of glass-forming liquids.^{18–20} We demonstrate that all these models of glass formation provide a quantitative description of segmental relaxation as a function of knot complexity, molecular mass, and temperature, despite their apparently distinct conceptual foundations. We then show that the extent of collective motion and the high frequency shear modulus in knotted ring polymer melts are closely interrelated, following the empirical relations established in our previous works based on linear polymer melts²² and the Kob-Andersen model system.²³ Finally, we discuss dynamic and elastic heterogeneities in relation to fragility and stiffness variations of knotted ring polymer melts, with a focus on how these trends relate to other glass-forming liquids where fragility is tuned over a large range.

2 Method

Our computational study is based on a generic, coarse-grained model of polymer melts.^{60,61} Since the model and simulation details have been provided at length in our previous work,⁵⁰ our description is brief here. Our simulated polymer melt is composed of N_p knotted rings of molecular mass M and knot complexity m_c , where M is the number of beads in a single chain and m_c is the minimum crossing number. N_p is adjusted for different M so that the total number of beads, $N = N_p M$, ranges from 8000 to 12800. The method for generating initial knot configurations is consistent with that of Vargas-Lara et al.,⁶² which employs Mathematica⁶³ to specify representative configurations for a prescribed knot topology (Figure 1).

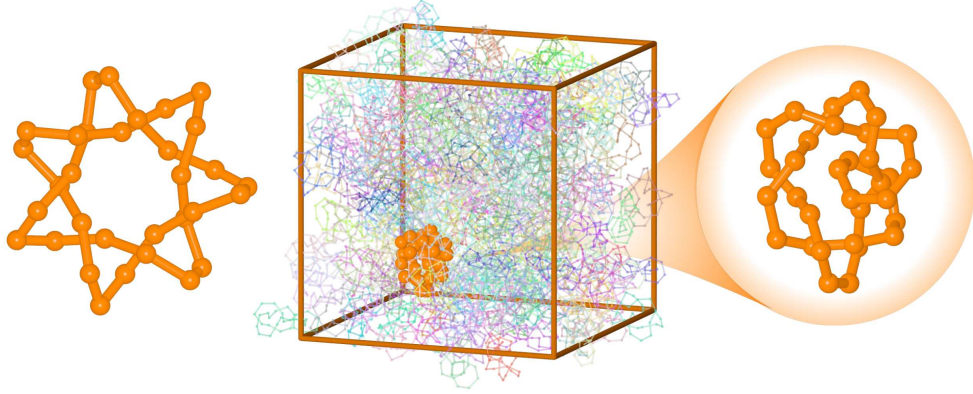


Figure 1: Example of a knotted ring polymer melt with the minimum crossing number of $m_c = 7$ and the molecular mass of $M = 32$. The left part illustrates the initial configuration of a knotted ring polymer. The right part displays a melt composed of 250 chains after equilibration, where one of the chains is highlighted and all the others are shown as translucent thin cylinders.

The present study deliberately selected prime knots with the subscript 1 (e.g., 3_1 , 4_1 , 5_1 , 6_1 , and 7_1) as research objects because they possess the highest symmetry within their respective crossing number classes. This high degree of symmetry makes them ideal benchmarks for establishing fundamental physical models. Notably, our selection already encompasses both torus (e.g., 3_1 , 5_1 , and 7_1) and twist knots (e.g., 4_1 and 6_1), which are the most representative knot families in polymer physics. While more subtle topological features, such as knot chirality or non-prime configurations, may introduce measurable differences in glass formation, our current findings suggest that the minimum crossing number m_c serves as the dominant descriptor for the observed “topological rigidification” across these different families. The exploration of how more complex topological details impact glass formation remains an interesting direction for future work.

The force field comprises two potentials. Nonbonded beads interact via a truncated-and-shifted Lennard-Jones (LJ) potential with an energy parameter ε , a length parameter σ , and a cutoff distance of $r_c = 2.5\sigma$. Chain connectivity is maintained by the finitely extensible nonlinear elastic (FENE) spring potential^{60,61} between adjacent beads, with a spring constant of $k_b = 30\varepsilon/\sigma^2$ and a maximum extension of $R_0 = 1.5\sigma$. All quantities

are reported in standard reduced LJ units; i.e., length, energy, temperature, and pressure are expressed in units of σ , ε , ε/k_B , and ε/σ^3 , respectively, where k_B is the Boltzmann constant. In addition, we define the time unit by $\tau = \sqrt{m_b\sigma^2/\varepsilon}$, where m_b is the bead mass. All our simulations were performed using the Large-scale Atomic/Molecular Massively Parallel Simulator (LAMMPS) package^{64,65} at zero pressure using a time step of $\Delta t = 0.005\tau$. Temperature and pressure were controlled via the Nosé-Hoover thermostat and barostat. Prior to data collection, the system was equilibrated for a duration significantly longer than its segmental structural relaxation time τ_α . Figure 1 shows an example of a knotted ring polymer melt composed of 250 chains with $m_c = 7$ and $M = 32$ after equilibration. We confirmed via an Alexander polynomial-based approach of Dai and coworkers⁶⁶ that the knot types generated initially remain unchanged after equilibration in our simulations. We refer the reader to ref 50 for additional technical details.

3 Results and Discussion

3.1 Overview of Structural Relaxation Time

Before assessing the validity of various models of glass formation in knotted ring polymer melts, we first review how basic relaxation properties are influenced by knot complexity and molecular mass. The quantity of primary interest here is the segmental structural relaxation time τ_α , which is obtained from the time (t) dependence of the self-intermediate scattering function $F_s(q, t)$. The wave number of $q^* = q = 7.0\sigma^{-1}$ is chosen to correspond to the first peak of the static structure factor $S(q)$ and thus to the typical intersegmental distance. τ_α is then defined by the time at which $F_s(q, t)$ decays to 0.1.⁵⁰ $F_s(q, t)$ also enables the definition of the non-ergodicity parameter f_{s,q^*} from $f_{s,q^*} = F_s(q, t = 1\tau)$,²² another quantity of interest, by adopting the caging onset time of $t_{\text{onset}} = 1\tau$. The specific definition of $F_s(q, t)$ is given in Section S1 of the Supporting Information, along with typical examples.

To frame our subsequent investigation below, Figure 2 summarizes the representative

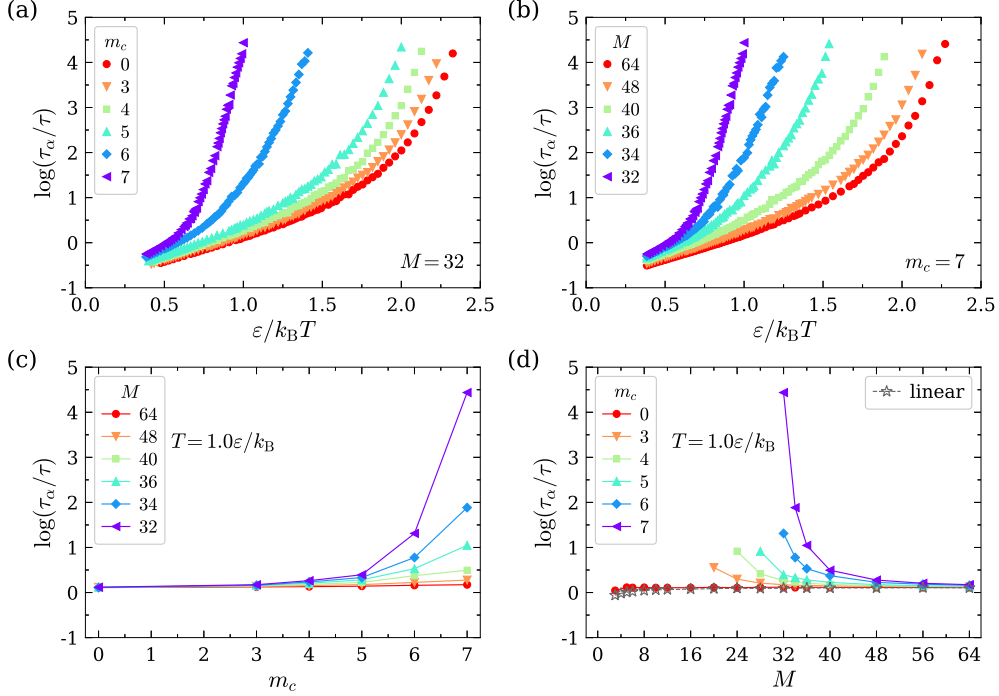


Figure 2: Structural relaxation time τ_α in variation with temperature T , knot complexity m_c , and molecular mass M . Panels (a) and (b) show $\log(\tau_\alpha/\tau)$ versus $\varepsilon/k_B T$ for a range of m_c at $M = 32$ and for a range of M at $m_c = 7$, respectively. Panels (c) and (d) show the variations with m_c and M of $\log(\tau_\alpha/\tau)$ over a range of fixed M and m_c at $T = 1.0\varepsilon/k_B$, respectively. The results for linear polymer melts are included as a reference in panel (d).

results for the variations of τ_α with T , m_c , and M . The T dependence of $\log(\tau_\alpha)$ is shown for a range of m_c at $M = 32$ and for a range of M at $m_c = 7$ in Figure 2a, b, respectively. We see that segmental dynamics slows down dramatically upon cooling and that both the magnitude and T dependence of τ_α can be affected strongly by knot complexity and molecular mass. Accordingly, our previous paper provided a detailed discussion of the variation of τ_α with m_c and M ,⁵⁰ along with the characteristic temperatures (such as T_g) and fragility of glass formation, as determined from the T dependence of τ_α . To examine the influence of knot complexity and molecular mass on τ_α at fixed T , Figure 2c indicates that τ_α initially changes with m_c weakly and then increases abruptly with further increasing m_c at about $m_c = 5$ in the low M regime, in line with the simulation results of Vargas-Lara et al.⁶² At sufficiently large M , however, knotting effects on τ_α are quite weak over the entire range of m_c considered in the present work. Concerning the M dependence of τ_α , a previous work

based on the same coarse-grained model showed that τ_α increases with increasing M in linear polymer melts at low T , while τ_α changes rather weakly with M in unknotted ring polymer melts.⁶⁷ In the presence of knots, however, τ_α is found to increase with decreasing M (Figure 2d). Indeed, our simulation results suggest that τ_α tends to diverge at a critically small M , a phenomenon that we plan to investigate thoroughly elsewhere. Notice that the temperature $T = 1.0\varepsilon/k_B$ is essentially in the Arrhenius regime at high T for linear polymer melts so that M dependence of τ_α is observed to be rather weak in Figure 2d.

The singular increase of τ_α with decreasing M at fixed m_c (Figure 2d) is particularly noteworthy. Our simulation results suggest that τ_α tends to diverge at a critically small M , a phenomenon that implies a transition toward a topologically induced dynamical arrest. We find that the M dependence of τ_α at fixed T can be reasonably described by an analogous Vogel-Fulcher-Tammann (VFT) functional form, $\tau_\alpha = \tau_0 \exp[D_M M_0 / (M - M_0)]$, where τ_0 is a prefactor, D_M quantifies the strength of the M dependence of τ_α , and M_0 is the molecular mass where τ_α extrapolates to infinity. This result implies that as the polymer chain length approaches the geometric limit required to maintain the knot, a topology-induced glass formation occurs. Evidently, this significant phenomenon is worthy of an extended discussion. This discussion requires us to carry out extended simulations at smaller M than those considered in the present work, where we focus on the knotted ring polymer melts upon cooling, a common route to glass formation. We plan to provide a more systematic scaling analysis and a thorough investigation of this critically small M regime in future work.

In previous works,^{50,62} the large variation of τ_α with m_c was attributed to “topological rigidification” induced by knots in the sense that chains are stiffened by knotting. Our previous systematic investigation of the conformational properties of knotted ring polymer melts⁵⁰ demonstrated that the persistence length and other size-related metrics undergo significant changes with varying m_c and M , providing a direct structural foundation for this mechanism. While such an idea is useful for understanding the general trends qualitatively, it remains unknown if a quantitative description of the segmental relaxation in knotted ring

polymer melts can be obtained based on the prevailing models of glass formation initially proposed for simpler systems such as the Kob-Andersen model system and linear polymer melts. Below, we discuss the effect of knotting on the extent of collective motion and material stiffness and examine the role of these properties in the quantitative description of the segmental structural relaxation time. This investigation is particularly worthwhile, given the fact that both T_g and fragility can be tuned over a large range by varying knot complexity and molecular mass.⁵⁰ In particular, we found that the characteristic temperatures of glass formation of knotted ring polymer melts, including T_g , increase progressively with increasing m_c , while the fragility of glass formation decreases progressively with increasing m_c under the condition of relatively small M . The decrease of fragility with increasing m_c was accompanied by a reduction of the dimensionless thermal expansion coefficient and isothermal compressibility, a general trend predicted by the GET.²⁵

3.2 String Model Description of Glass Formation

Dynamic heterogeneity is a universal feature of glass-forming liquids upon cooling toward T_g . This phenomenon is characterized by the formation of spatially correlated regions with markedly different dynamics in that some regions are composed of relatively mobile or fast particles, while particles in other complementary regions display significantly lower mobility. This widely observed phenomenon is also regarded as being the key to understanding the anomalous physical properties of glass-forming materials. Moreover, extensive simulations^{15,21,68-74} have revealed that the most mobile particles move cooperatively in a stringlike fashion. Such stringlike cooperative motion has been shown to provide a quantitative realization of the hypothetical “cooperatively arranging regions” (CRR) in the AG model.⁹

We follow the established procedure for polymeric systems to quantify the stringlike cooperative motion and determine the average string length L .^{69,72} Details can be found in Section S1 of the Supporting Information. Mirroring our discussion of τ_α in Section 3.1,

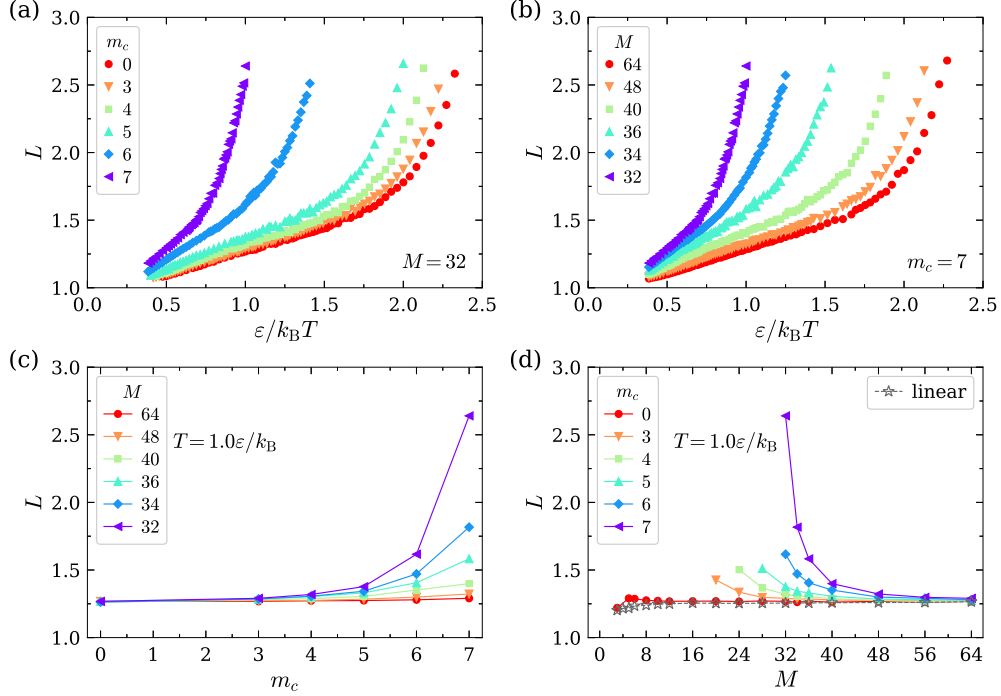


Figure 3: Average string length L in variation with temperature T , knot complexity m_c , and molecular mass M . Panels (a) and (b) show L versus $\varepsilon/k_B T$ for a range of m_c at $M = 32$ and for a range of M at $m_c = 7$, respectively. Panels (c) and (d) show the variations with m_c and M of L over a range of fixed M and m_c at $T = 1.0\varepsilon/k_B$, respectively. The results for linear polymer melts are included as a reference in panel (d).

Figure 3 summarizes the representative results for the variations of L with T , m_c , and M . We find that L exhibits similar trends to those of τ_α . The T dependence of L is presented for a range of m_c at $M = 32$ and for a range of M at $m_c = 7$ in Figure 3a, b. These results demonstrate that both m_c and M can likewise influence L quite strongly. Specifically, Figure 3c indicates that L varies weakly with m_c when m_c is small, but significant changes occur when m_c is increased to 5 in the low M regime. However, when M is large, the variation of L with m_c remains weak across the entire range of m_c considered. Additionally, Figure 3d indicates that L gradually increases as M decreases, which is different from the trends for linear and unknotted ring polymer melts. These results imply that the extent of cooperative motion can be tuned by knots over a wide range.

The string model of glass formation is built upon the finding that stringlike cooperative motion L provides a reasonable realization of the abstract CRR in the AG model.⁹ The

validity of the string model has been supported by studies based on a range of polymeric and other glass-forming systems.^{15,21,73–80} The string model finds further theoretical justification in the analysis of Freed,¹⁴ who extended transition state theory (TST)^{81,82} to account for such stringlike cooperative barrier-crossing events in glass-forming liquids.

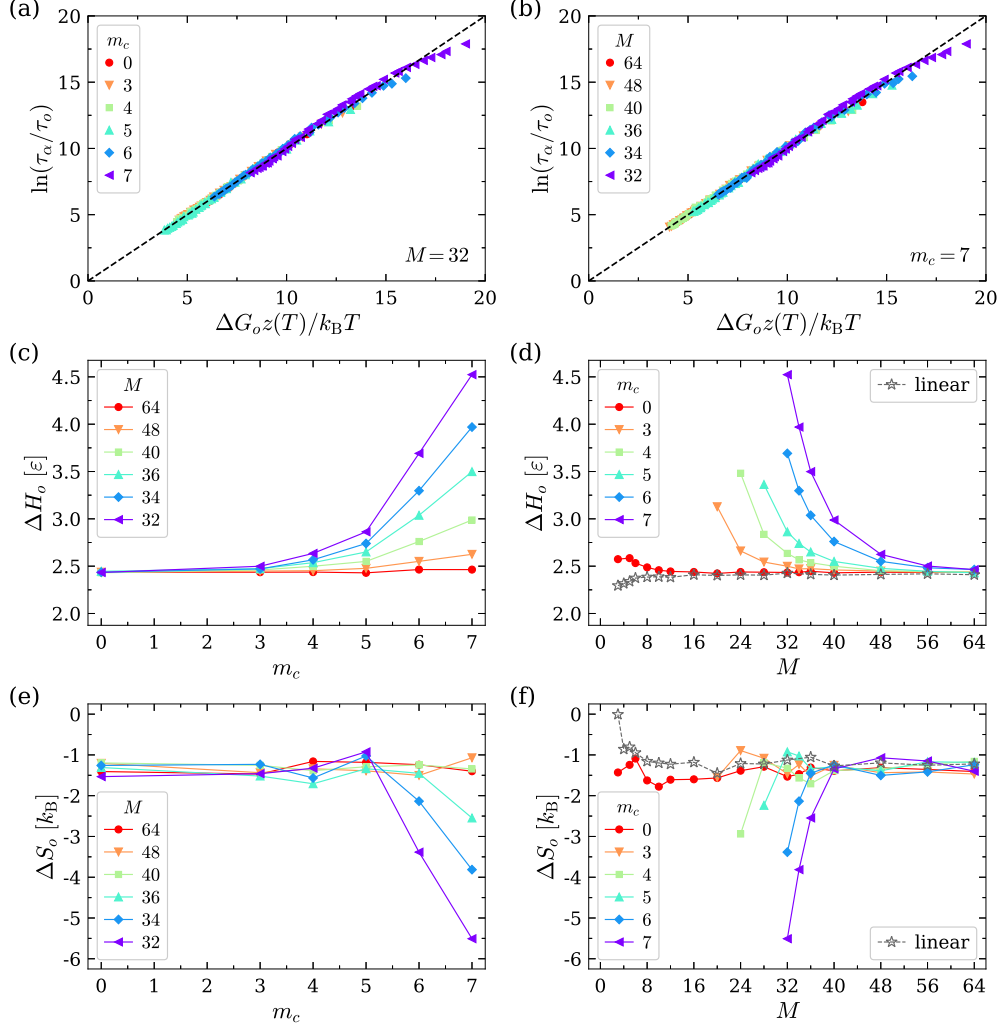


Figure 4: String model description of glass formation. Panels (a) and (b) show $\ln(\tau_\alpha/\tau_o)$ versus $\Delta G_{oz}(T)/k_B T$ for a range of m_c at $M = 32$ and for a range of M at $m_c = 7$, respectively. Dashed lines indicate $\ln(\tau_\alpha/\tau_o) = \Delta G_{oz}(T)/k_B T$, where τ_o , L_A , and ΔG_o are explained in the text. Panels (c–f) show the variations with m_c and M of the activation enthalpy ΔH_o and entropy ΔS_o over a range of fixed M and m_c , respectively. The results for linear polymer melts are included as a reference in panels (d) and (f).

To describe the dynamics below the onset temperature T_A , where relaxation starts to become overtly non-Arrhenius, the string model assumes that the activation free energy

$\Delta G(T)$ for structural relaxation is proportional to a factor $z(T)$ given by the average string length $L(T)$ at a given T normalized by its value L_A at T_A , $z(T) = L(T)/L_A$. (A detailed discussion of T_A for the present knotted ring polymer melts can be found in our previous paper.⁵⁰) This assumption yields a temperature-dependent activation free energy $\Delta G(T) = \Delta G_o z(T)$, where ΔG_o is the high-temperature activation free energy, taking the form of $\Delta G_o = \Delta H_o - T\Delta S_o$ with the enthalpic ΔH_o and entropic ΔS_o contributions. The string model then yields the following expression for τ_α ,

$$\tau_\alpha = \tau_o \exp \left[\frac{\Delta G_o}{k_B T} z(T) \right], \quad z(T) = L(T)/L_A \quad (1)$$

The parameter τ_o can be eliminated by using the value of τ_α at T_A , and ΔH_o can be determined from the Arrhenius fit of the T dependence of τ_α in the high-temperature regime, as discussed in our previous paper.⁵⁰ These considerations result in the following equation, with ΔS_o being the only fitting parameter,

$$\tau_\alpha = \tau_\alpha(T_A) \exp \left[\frac{\Delta H_o - T\Delta S_o}{k_B T} z(T) - \frac{\Delta H_o - T_A\Delta S_o}{k_B T_A} \right] \quad (2)$$

We use the above equation to test the validity of the string model. As illustrated in Figure 4a, b, all our simulation data, spanning a range of T , m_c , and M , can be satisfactorily described by eq 2. This finding implies that the pronounced variations of τ_α with m_c and M can indeed be understood based on the extent of stringlike cooperative motion.

We summarize the fitted activation parameters ΔH_o and ΔS_o in Figure 4c-f. In previous works based on other polymeric systems,^{21,22,73,74} ΔH_o and ΔS_o were often found to vary proportionally, an effect known as the entropy-enthalpy compensation.^{83,84} Our previous simulation works also showed strong positive correlations in polymer melts with variable cohesive energy⁸⁵ and pressure,⁸⁶ but a negative correlation observed in polymer melts with varying chain stiffness is evidently not “universal”.⁸⁷ Our analysis in Figure 4 indicates that there is a correlation between ΔH_o and ΔS_o in knotted ring polymer melts, despite the

absence of a universal relationship.

3.3 Localization Model Description of Glass Formation

After showing that the segmental relaxation in knotted ring polymer melts can be understood based on the stringlike cooperative motion, we examine whether or not other theoretical frameworks provide a reasonable description of the same phenomenon. More specifically, this section considers the localization model of glass formation, another framework that has attracted considerable interest recently.^{16,17,21} The localization model links the structural relaxation time τ_α to the Debye-Waller parameter $\langle u^2 \rangle$. This quantity defines a measure of local stiffness and can be determined by the mean square displacement (MSD) on a caging time scale on the order of a picosecond.^{88–91} The definition of the MSD can be found in Section S1 of the Supporting Information, along with typical examples. $\langle u^2 \rangle$ can be regarded as a measure of the dynamical free volume and thus provides insights into local mobility gradients that are not evident from a structural perspective.⁹² Moreover, $\langle u^2 \rangle$ has been linked to atomic-scale stiffness and the overall shear modulus of the entire material, offering insight into local fluctuations and deformation of glass-forming materials.⁹³ We discuss this point in further detail in Section 3.7. Since the non-ergodicity parameter f_{s,q^*} also provides a measure of material stiffness,²² the relationship between f_{s,q^*} and $\langle u^2 \rangle$ in knotted ring polymer melts is briefly discussed in the Section S2 of the Supporting Information.

We first discuss the variations of $\langle u^2 \rangle$ with T , m_c , and M in knotted ring polymer melts, as given in Figure 5. Again, we see that both m_c and M can substantially influence the magnitude of $\langle u^2 \rangle$. As shown in Figure 5c, the dependence of $\langle u^2 \rangle$ on m_c is generally weak, except for a pronounced decrease when m_c is raised to 5 in the low M regime. In contrast, when M is large, the variation of $\langle u^2 \rangle$ with m_c remains weak across the entire range of m_c considered. Furthermore, Figure 5d demonstrates that $\langle u^2 \rangle$ gradually decreases as M decreases, a trend that deviates from those for linear and unknotted ring polymer melts. Overall, when T , m_c , and M are varied, $\langle u^2 \rangle$ exhibits similar trends to those discussed above

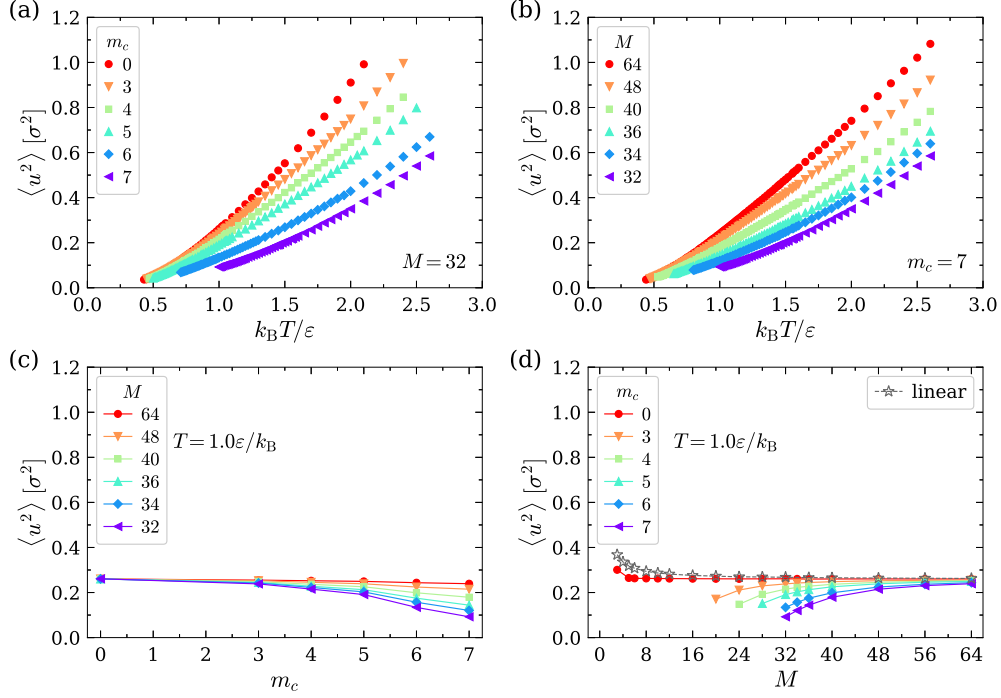


Figure 5: Debye-Waller parameter $\langle u^2 \rangle$ in variation with temperature T , knot complexity m_c , and molecular mass M . Panels (a) and (b) show $\langle u^2 \rangle$ versus $k_B T / \epsilon$ for a range of m_c at $M = 32$ and for a range of M at $m_c = 7$, respectively. Panels (c) and (d) show the variations with m_c and M of $\langle u^2 \rangle$ over a range of fixed M and m_c at $T = 1.0\epsilon/k_B$, respectively. The results for linear polymer melts are included as a reference in panel (d).

for τ_α and L . It is then of interest to explore the possibility of a quantitative connection between τ_α and $\langle u^2 \rangle$.

The original formulation of the localization model proposes that τ_α should be related to $\langle u^2 \rangle$ by the following relation,

$$\tau_\alpha = \tau_u \exp \left[(u_0^2 / \langle u^2 \rangle)^{\alpha/2} \right] \quad (3)$$

where the parameters τ_u and u_0^2 can be specified in terms of the simulation data for τ_α and $\langle u^2 \rangle$ at T_A , namely, $\tau_A = \tau_\alpha(T_A)$ and $u_A^2 = \langle u^2(T_A) \rangle$, and α is an adjustable parameter in the model discussed below. The localization model then adopts the remarkably simple relation,

$$\tau_\alpha = \tau_A \exp \left[(u_A^2 / \langle u^2 \rangle)^{\alpha/2} - 1 \right] \quad (4)$$

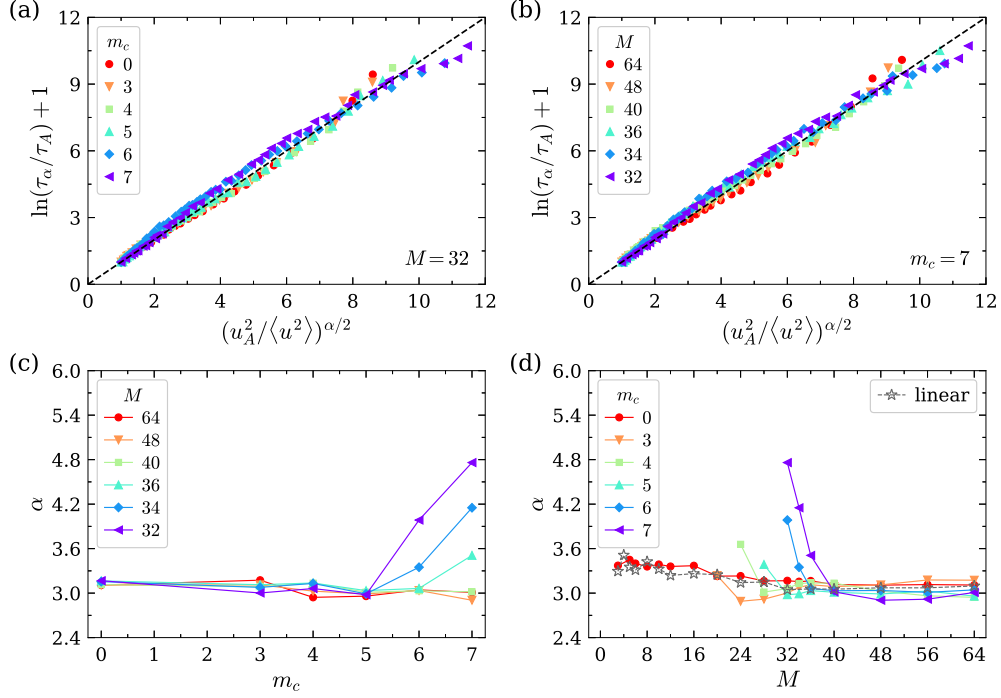


Figure 6: Localization model description of glass formation. Panels (a) and (b) show $\ln(\tau_\alpha/\tau_A) + 1$ versus $(u_A^2/\langle u^2 \rangle)^{\alpha/2}$ for a range of m_c at $M = 32$ and for a range of M at $m_c = 7$, respectively. Dashed lines indicate $\ln(\tau_\alpha/\tau_A) + 1 = (u_A^2/\langle u^2 \rangle)^{\alpha/2}$, where τ_A , u_A^2 , and α are explained in the text. Panels (c) and (d) show the variations with m_c and M of α over a range of fixed M and m_c , respectively. The results for linear polymer melts are included as a reference in panel (d).

A test of the localization model of glass formation is shown in Figure 6a, b, where we find that this model provides a satisfactory description of our simulation data for knotted ring polymer melts. Figure 6c shows the variation of α with m_c . It can be seen that α remains relatively constant for large values of M as m_c changes, while for smaller values of M , α initially remains unchanged in magnitude with respect to m_c , but α exhibits a significant increase at $m_c = 5$ to values that evidently exceed 3. Figure 6d illustrates the variation of α with M . For small m_c , α for knotted ring polymer melts depends weakly on M , similar to that of linear and unknotted ring polymers, but α increases with decreasing M when m_c is large.

Remarkably, the localization model involves no free parameter if the exponent α is taken to be the spatial dimensionality d so that $\langle u^2 \rangle^{\alpha/2}$ has the units of volume. In the original

investigation of the localization model computational by Starr and coworkers,^{21,94,95} the dependence of τ_α on $\langle u^2 \rangle$ for model polymer melts indicated an exponent consistent with $\alpha = 3$. Later extensive simulations of the Kob-Andersen model system under a wide range of densities and pressures as well as a Zr-Cu metallic glass also indicated consistency with $\alpha = 3$.^{17,23} Additionally, it was found that the interfacial dynamics of both crystalline and metallic glass-forming materials can be well described by the localization model with $\alpha = 3$.^{96,97} Despite the fact that α has often been found to be near 3, there have also been reports of apparent α values differing appreciably from 3.^{16,98,99} In our previous work on the Kob-Andersen model system,²³ we also found that α could vary over an appreciable range until we realized that the choice of time at which $\langle u^2 \rangle$ is defined can exert an appreciable influence on α and that the uncertainty in the estimation of T_A can also influence the apparent value of α . By applying a physically robust criterion, where t_{onset} corresponds to the timescale at which the fast β - and α -relaxation processes merge, we confirm that while the choice of t_{onset} can shift the absolute magnitude of α , the qualitative trend of α increasing above 3 in the “tight knot” limit remains robust. This observation aligns with recent theoretical reformulations of the localization model,¹⁰⁰ suggesting that α is not a universal constant, but rather a variable reflecting the degree of anharmonicity of intermolecular interactions. To quantitatively test this link between the non-universal behavior of α and the nature of particle localization in knotted polymers, we next analyze the degree of non-linearity in the T dependence of $\langle u^2 \rangle$, which serves as a practical measure of intermolecular anharmonicity.

To illustrate this effect, we first calculated $\langle u^2 \rangle$ for our polymer melts based on the assumption that the characteristic time scale for defining $\langle u^2 \rangle$ was equal to 1τ . This reduced time corresponds to a time scale on the order of a picosecond in laboratory units, which is a convention used in previous simulations of polymer liquids¹⁰¹ and this time scale serves as a good approximation of the α -relaxation time at T_A for our model polymer melts. Yuan et al.^{23,102} have strongly advocated that $\tau_\alpha(T_A)$ is the appropriate definition of the caging onset time scale defining $\langle u^2 \rangle$ based on a thorough analysis of the Kob-Andersen model system.

In Section S3 of the Supporting Information, we also show a test of the localization model based on the alternative assumption of a caging onset time, $t_{\text{onset}} = 2\tau$. Indeed, this larger choice of t_{onset} leads to values of α closer to 2.5 for linear and unknotted polymer melts. Our estimates of α based on the criterion $t_{\text{onset}} = 1\tau$, which we think is a more suitable criterion, are shown in Figure 6c, d.

Our results in Figure 6c, d reveal an unexpected trend in α , with increasing m_c and in the limit of “tight” knots having low M where there seems to be a real trend for α to approach values larger than 3. (The same qualitative increase is also apparent in α estimates based on $t_{\text{onset}} = 2\tau$.) This trend in α looks convincing, so the generality of $\alpha = 3$ is clearly suspect. The source of this variability of α then requires a discussion based on existing formulations of the localization model.

Simmons et al.¹⁶ heuristically argued in an early formulation of the localization model that the volume dynamically explored by chain segments in complex fluids, such as polymer melts, could lead to anisotropic, thread-like dynamical free volume regions instead of compact quasi-spherical regions. Based on this physical model, it was then suggested that this effect could plausibly result in values of the effective dimension parameter α being less than the spatial dimensionality d , and that anisotropy of the dynamical free volume regions could naturally explain some potential variability of α with the fluid type. Unfortunately, the physically appealing geometrical model of the dynamical free volume “structure” cannot explain values of α larger than 3 in three-dimensional simulations, as reported in some previous simulations noted above and in Figure 6, depicting our simulations for ring polymer melts of variable m_c and M . Evidently, this model of α variability is simply not adequate to explain observed trends in apparent α values. As noted previously, Douglas et al.¹⁰⁰ reformulated the localization model based on a general, but rather abstract dynamical systems perspective. The magnitude of α is predicted to vary in this formulation, but its value reflects the degree of anharmonicity of the intermolecular interaction, making it difficult to estimate the precise value of α for any particular molecular fluid. On the other hand, it is

possible to gain qualitative insight into the variation of α in fluids through the quantification of the degree of non-linearity in the T dependence of $\langle u^2 \rangle$, a well-known practical measure of the anharmonicity of the intermolecular interaction.^{101,103}

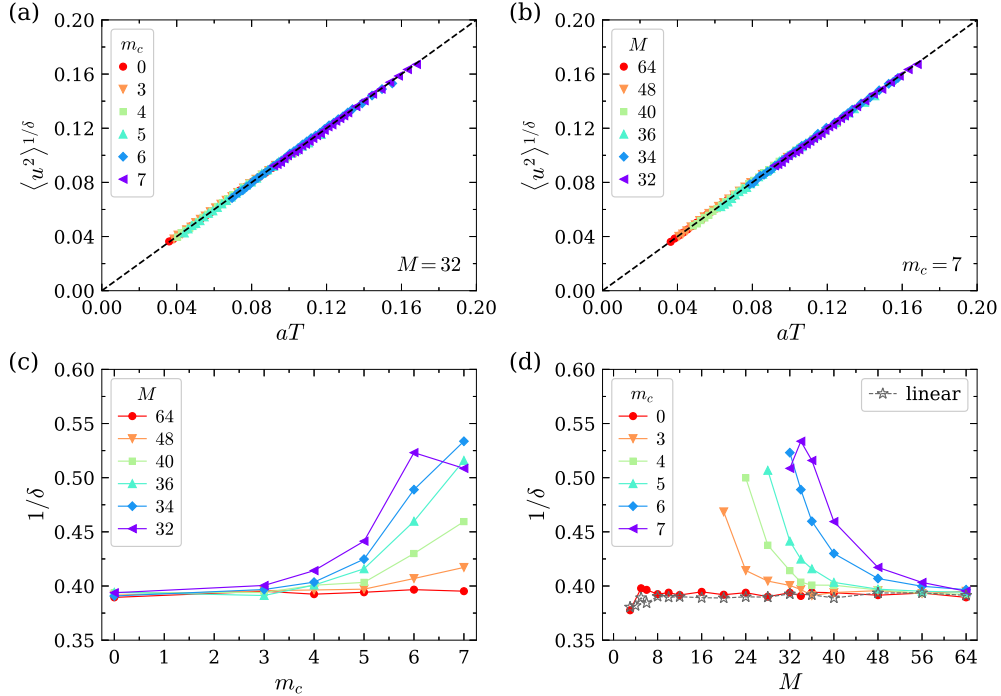


Figure 7: Analysis of the temperature dependence of the Debye-Waller parameter $\langle u^2 \rangle$. Panels (a) and (b) show $\langle u^2 \rangle^{1/\delta}$ versus aT for a range of m_c at $M = 32$ and for a range of M at $m_c = 7$, respectively. Dashed lines indicate $\langle u^2 \rangle^{1/\delta} = aT$, where δ and a are fitting parameters that depend on m_c and M . Panels (c) and (d) show the variations with m_c and M of $1/\delta$ over a range of fixed M and m_c , respectively. The results for linear polymer melts are included as a reference in panel (d).

Betancourt et al.¹⁰¹ introduced a convenient method for quantifying the nonlinear T dependence of $\langle u^2 \rangle$, through the nonlinear transformation, $\langle u^2 \rangle^{1/\delta} \sim T$, where δ is an “anharmonicity parameter”, given that a linear T scaling of $\langle u^2 \rangle$ is characteristic of harmonically localized particles. The use of such non-linear scaling of $\langle u^2 \rangle$ to characterize material anharmonicity has been established in early studies of various condensed systems.^{104–106} Notably, this method can apparently be applied readily to essentially any fluid. Accordingly, we analyze the influence of m_c and M on the degree of anharmonicity based on such a method which has not been applied to any specific purpose previously. Figure 7a, b indicates that

a linear relation between $\langle u^2 \rangle^{1/\delta}$ and T generally holds quite well in knotted ring polymer melts. Figure 7c, d summarizes the fitted results for $1/\delta$ as a function of m_c and M . As can be seen, the degree of anharmonicity δ increases with increasing m_c for small M and with decreasing M for large m_c , exhibiting the same general trends for α observed in Figure 6c, d. In the case of $M = 32$ and $m_c = 7$, $1/\delta$ exhibits a nonmonotonic variation, which might arise from non-equilibrium effects associated with knot rigidification in these limits.

Although it would be truly remarkable if the structural relaxation time τ_α can be predicted based on $\langle u^2 \rangle$ estimates for all fluids without any free parameters, as followed from the localization model when α equals 3, there is apparently some variability in the exponent α for some systems that can spoil this “universality”. The model of knotted ring polymers has allowed us to probe this non-universality and gain insight into its cause.

3.4 Shoving Model Description of Glass Formation

In addition to the string and localization models, there are alternative models of liquid dynamics characterized by fundamentally different quantities. This section focuses on the shoving model, which attributes the dramatic slowdown of structural relaxation and diffusion in glass-forming materials to the increase in shear modulus or other measures of material stiffness. The glassy plateau shear modulus G_p is often measured as the high-frequency shear modulus in viscoelastic materials since the measurements of material stiffness have been suggested to determine the temperature-dependent activation free energy $\Delta G(t)$ of glass-forming liquids.^{9,15,25,72} Specifically, G_p is estimated from the stress autocorrelation function $G(t)$ at the caging onset time, i.e., $G_p \equiv G(t = 1\tau)$, as in the case of $\langle u^2 \rangle$ and f_{s,q^*} , while the infinite-frequency modulus is given by $G_\infty = G(t \rightarrow 0^+)$. The definition of $G(t)$ can be found in Section S1 of the Supporting Information, along with typical examples.

Figure 8 summarizes the representative results for the variations of G_p with T , m_c , and M . It is clear that G_p follows analogous patterns to those observed for τ_α , L , and $\langle u^2 \rangle$. The relationship between G_p and T is illustrated in Figure 8a for varying m_c at $M = 32$, and

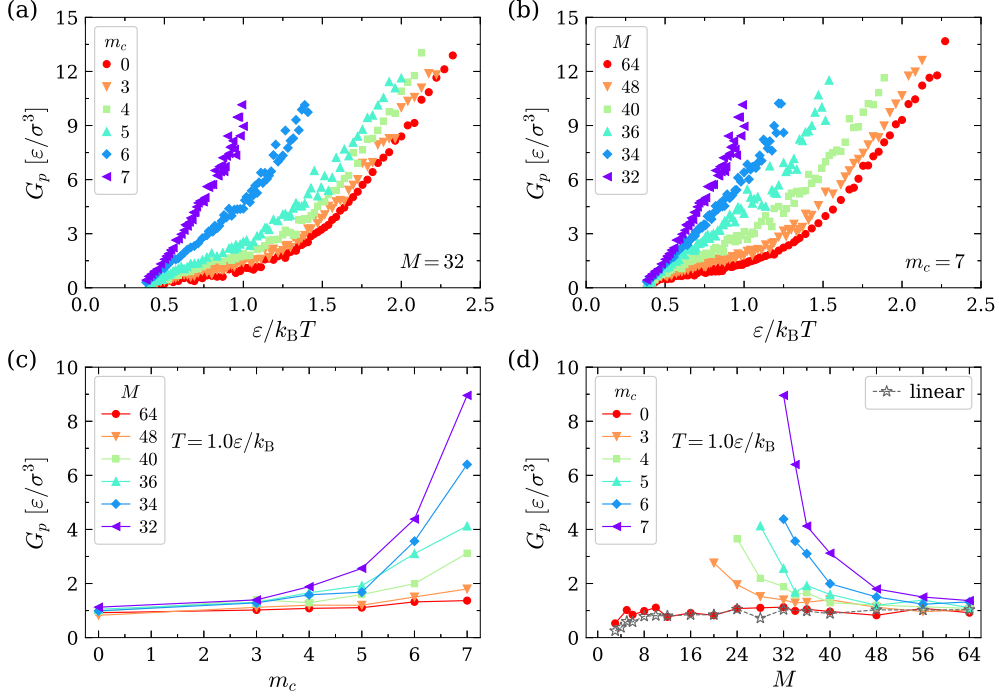


Figure 8: Glassy plateau shear modulus G_p in variation with temperature T , knot complexity m_c , and molecular mass M . Panels (a) and (b) show G_p versus $\varepsilon/k_B T$ for a range of m_c at $M = 32$ and for a range of M at $m_c = 7$, respectively. Panels (c) and (d) show the variations with m_c and M of G_p over a range of fixed M and m_c at $T = 1.0\varepsilon/k_B$, respectively. The results for linear polymer melts are included as a reference in panel (d).

in Figure 8b for varying M at $m_c = 7$. These findings indicate that both m_c and M can markedly affect G_p . To investigate the effects of m_c and M on G_p at a constant T , Figure 8c reveals that G_p initially exhibits a weak dependence on m_c , followed by a large increase around $m_c = 5$ in the low M regime. At sufficiently high M , the influence of knotting on G_p remains minimal across the entire range of m_c examined in this study, with results aligning well with those of linear and unknotted ring polymers. Note that our simulation data for G_p are more scattered than the other data such as τ_α , L , and $\langle u^2 \rangle$, because the stress autocorrelation function is a property of the overall system that cannot be averaged over individual particles.

We now examine the extent to which structural relaxation can be described by the showing model. A key prediction of this model is that structural relaxation is activated by an energy barrier ΔE , which is proportional to an elastic modulus explicitly identified as the

instantaneous shear modulus G_{inst} due to the cage breaking,

$$\tau_\alpha = \tau_G \exp(\Delta E/k_B T), \quad \Delta E = G_{\text{inst}} V_c^* \quad (5)$$

where τ_G is a prefactor and V_c^* is an empirical characteristic volume, which is assumed to be on the order of a segment volume and independent of T . Puosi and Leporini¹⁰⁷ first emphasized that G_{inst} should not be identified with the infinite frequency shear modulus, G_∞ , which has a well-known thermodynamic definition. Instead, G_∞ should be associated with a glassy plateau modulus G_p , corresponding to $G(t)$ after an initial fast β stress relaxation process, as discussed above. Since the fast β -relaxation time is generally on the order of 0.1 to 1 ps for both molecular and atomic glass-forming liquids,^{101,108,109} our definition of G_p at $t = 1\tau$ is consistent with this picture. The qualitative difference between G_p and G_∞ has been noted previously.^{107,110} Dyre and Wang¹⁹ accordingly modified the shoving model by replacing G_∞ with G_p .

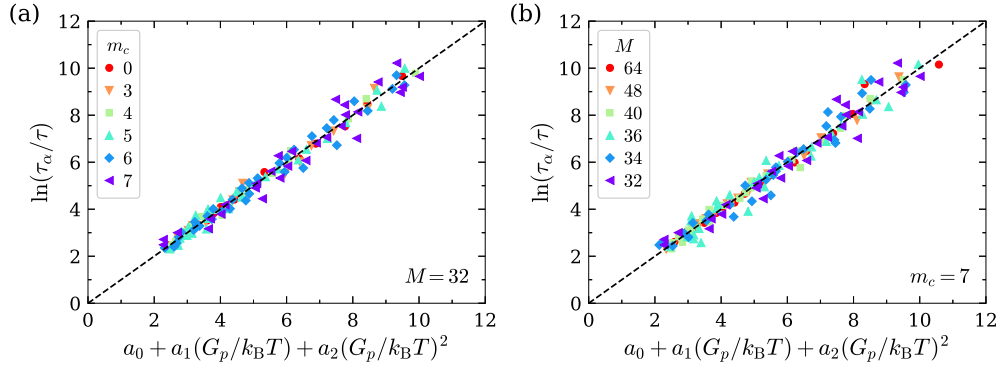


Figure 9: Shoving model description of glass formation. Panels (a) and (b) show $\ln(\tau_\alpha/\tau)$ versus $a_0 + a_1(G_p/k_B T) + a_2(G_p/k_B T)^2$ for a range of m_c at $M = 32$ and for a range of M at $m_c = 7$, respectively. a_0 , a_1 , and a_2 are fitting parameters that depend on m_c and M . Lines indicate $\ln(\tau_\alpha/\tau) = a_0 + a_1(G_p/k_B T) + a_2(G_p/k_B T)^2$.

Puosi and Leporini¹⁰⁷ further proposed a specific quadratic relationship between τ_α and G_p , which was verified for coarse-grained polymer melts and small-molecule liquids,

$$\ln(\tau_\alpha) = a_0 + a_1(G_p/k_B T) + a_2(G_p/k_B T)^2 \quad (6)$$

where a_0 , a_1 , and a_2 are adjustable constants. Our recent work also showed that the same functional form holds in the Kob-Andersen model system over a wide range of densities and pressures.²³ Here, we test such a relation for knotted ring polymer melts with different m_c and M . As can be seen in Figure 9, eq 6 holds reasonably well, although the simulation data are scattered when the knots are tight, due to the reason explained above.

3.5 Property Interrelations

The near equivalence of independent approaches to describing the dynamics of glass-forming liquids, each centering around different fluid properties, has interesting implications. In particular, this finding implies that the properties emphasized by these approaches might be closely interrelated. In this section, we show that it is indeed the case in knotted ring polymer melts.

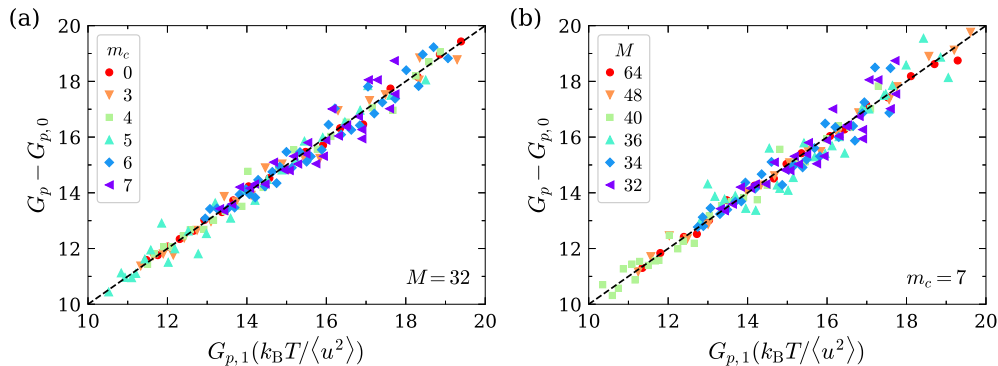


Figure 10: Correlation between the Debye-Waller parameter $\langle u^2 \rangle$ and the glassy plateau shear modulus G_p . Panels (a) and (b) show $G_p - G_{p,0}$ versus $G_{p,1}(k_B T / \langle u^2 \rangle)$ for a range of m_c at $M = 32$ and for a range of M at $m_c = 7$, respectively. $G_{p,0}$ and $G_{p,1}$ are fitting parameters that depend on m_c and M . Lines indicate $G_p - G_{p,0} = G_{p,1}(k_B T / \langle u^2 \rangle)$.

One nontrivial property interrelation is that between the high frequency modulus G_p of the entire material and $\langle u^2 \rangle$, a molecular scale measure of material stiffness. In particular, previous works have established the nontrivial relation,^{107,111}

$$G_p \approx G_{p,0} + G_{p,1}(k_B T / \langle u^2 \rangle) \quad (7)$$

where $G_{p,0}$ and $G_{p,1}$ are material-dependent constants. This remarkable relation has been confirmed for many materials,^{22,93,111–113} and in Figure 10, we show that eq 7 is also applicable to knotted ring polymer melts, where the constants $G_{p,0}$ and $G_{p,1}$ depend on m_c and M . This relation also enables an investigation of the *local* stiffness of a material based on the distribution of $\langle u^2 \rangle$, namely, the elastic heterogeneity, as discussed in Section 3.7. It has been established that the bulk modulus,^{112–116} central to some models of the dynamics of condensed materials,¹¹⁷ and the configurational entropy S_c ,^{23,114} central to the AG model of glass formation,⁹ can also be related to $\langle u^2 \rangle$ quantitatively.

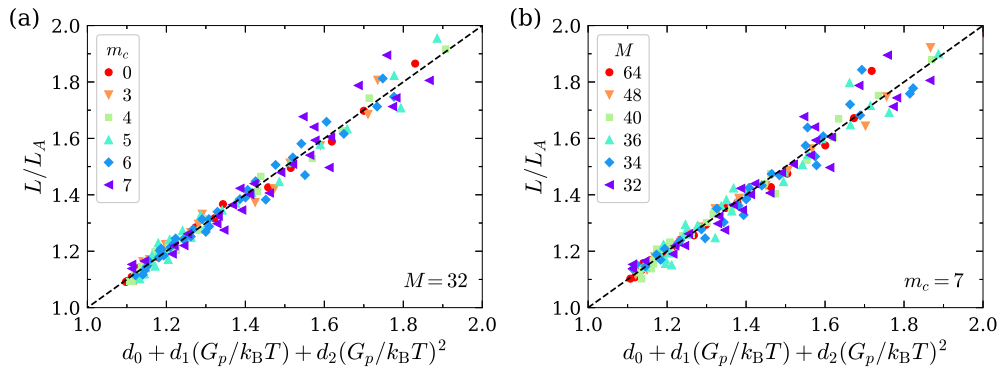


Figure 11: Correlation between the glassy plateau shear modulus G_p and the extent of collective motion L/L_A . Panels (a) and (b) show L/L_A versus $d_0 + d_1(G_p/k_B T) + d_2(G_p/k_B T)^2$ for a range of m_c at $M = 32$ and for a range of M at $m_c = 7$, respectively. d_0 , d_1 , and d_2 are fitting parameters that depend on m_c and M . Lines indicate $L/L_A = d_0 + d_1(G_p/k_B T) + d_2(G_p/k_B T)^2$.

Another nontrivial correspondence of particular interest is the relation between cooperative motion and rigidity in knotted polymers, a phenomenon discussed speculatively by de Gennes.¹¹⁸ Based on the results discussed above for the string and shoving models, we discuss this type of relation in knotted ring polymer melts. In particular, we may expect a direct scaling relationship between the glassy plateau shear modulus G_p and the extent of collective motion L/L_A , a relationship considered previously in linear polymer melts.²² Reminiscent of the functional form of eq 6, we find in Figure 11 that a quadratic relation

describes the relationship between L and G_p quite well in knotted polymer melts,

$$L/L_A = d_0 + d_1(G_p/k_B T) + d_2(G_p/k_B T)^2 \quad (8)$$

where d_0 , d_1 , and d_2 are fitting parameters. This scaling reflects the parallel emergence of rigidity and collective motion that underlies applicability of both the string and shoving models to the dynamics of glass-forming liquids. This relation between collective motion and stiffness can also be considered by applying the same analysis to individual knotted polymers, which we plan to perform in future work.

3.6 Dynamic Heterogeneity

It is now well established that the dynamics of glass-forming liquids become increasingly spatially heterogeneous upon approaching T_g . In Section 3.2, we discuss the role of stringlike cooperative motion in understanding the segmental relaxation of knotted ring polymer melts, which represents one specific characterization of dynamic heterogeneity. Here, we examine dynamic heterogeneity from other complementary perspectives. In particular, we focus on the non-Gaussian parameter $\alpha_2(t)$, which characterizes the dynamic heterogeneity associated with mobile particles, because our previous works identified an intriguing relation between this quantity and the relaxation time in the Kob-Andersen model system.²³ $\alpha_2(t)$ displays a primary peak, denoted as α_2^* , at a peak time t^* , which is related to the lifetime of the mobile particle clusters.^{72,80} The definition of $\alpha_2(t)$ can be found in Section S1 of the Supporting Information, along with typical examples.

Although the non-Gaussian parameter is commonly interpreted as a measure of the extent of dynamic heterogeneity, its precise physical meaning remains somewhat obscure, beyond the observation that this peak occurs at a characteristic time t^* at which the size of the mobile particle clusters peaks.⁷² A potential approach provides some insight into how the magnitude of “dynamic heterogeneity”, as quantified by α_2^* , relates to the magnitude of the

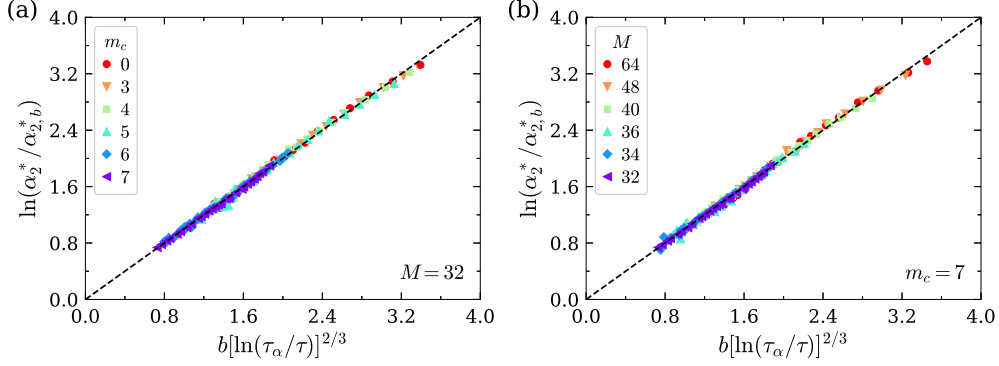


Figure 12: Relation between the structural relaxation time τ_α and the peak magnitude α_2^* of the non-Gaussian parameter. Panels (a) and (b) show $\ln(\alpha_2^*/\alpha_{2,b}^*)$ versus $b[\ln(\tau_\alpha/\tau)]^{2/3}$ for a range of m_c at $M = 32$ and for a range of M at $m_c = 7$, respectively. $\alpha_{2,b}^*$ and b are fitting parameters that depend on m_c and M . Lines indicate $\ln(\alpha_2^*/\alpha_{2,b}^*) = b[\ln(\tau_\alpha/\tau)]^{2/3}$.

structural relaxation time τ_α , as gleaned from the striking correlative relation,²³

$$\ln(\alpha_2^*/\alpha_{2,b}^*) = b[\ln(\tau_\alpha/\tau)]^{2/3} \quad (9)$$

where $\alpha_{2,b}^*$ and b are fitting parameters, as identified in a previous study.²³ We take this opportunity to test the generality of this relation for knotted ring polymer melts with different m_c and M . As can be seen in Figure 12, the relation given by eq 6 also holds quite well. It is emphasized that there is currently no theoretical understanding of this striking relationship between α_2^* and τ_α . We develop this expression further by combining it with the string model of glass formation, as discussed in Section 3.2.

It is a longstanding belief that the fragility of glass formation is somehow related to the extent of dynamic heterogeneity, but any such general relation has remained elusive. We may obtain a direct relation formally through the combination of eq 1, which relates τ_α to L , and eq 9, which relates α_2^* to τ_α . We show the result of combining these relations in Figure 13, where we see a scaling of α_2^* with the extent of collective motion $z(T)$ in knotted ring polymer melts. A recent work based on the GET has indicated that the segmental fragility m is directly related to $z(T_g)$ for a wide range of polymer models,¹¹⁹ i.e., $m \approx 7.9 \exp[0.6z(T_g)]$, so we formally have a relation between the dynamic heterogeneity measure α_2^* and the

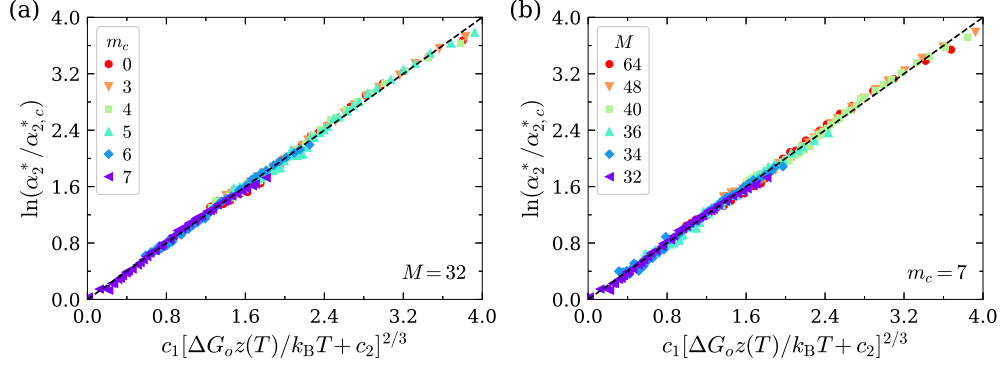


Figure 13: Relation between the extent of stringlike collective motion $z(T)$ and the peak magnitude α_2^* of the non-Gaussian parameter. Panels (a) and (b) show $\ln(\alpha_2^*/\alpha_{2,c}^*)$ versus $c_1 [\Delta G_o z(T)/k_B T + c_2]^{2/3}$ for a range of m_c at $M = 32$ and for a range of M at $m_c = 7$, respectively. $\alpha_{2,c}^*$, c_1 and c_2 are fitting parameters that depend on m_c and M . Lines indicate $\ln(\alpha_2^*/\alpha_{2,c}^*) = c_1 [\Delta G_o z(T)/k_B T + c_2]^{2/3}$.

fragility of glass formation when α_2^* is extrapolated to T_g .

While we do not possess a theoretical framework that allows us to understand exactly in what sense $\alpha_2(t)$ is a measure of dynamic heterogeneity, the above correlations suggest that a deeper understanding of these scaling relationships might offer new and general insights into glass formation.

3.7 Elastic Heterogeneity

Elastic heterogeneity is a phenomenon naturally arising from the expectation that the mobile and immobile regions are associated with long-lived domains exhibiting distinct stiffness characteristics.¹¹² Following the recent works of Zheng et al.^{112,113} and Wang et al.,⁹³ we adopt eq 7 as the defining relationship for local material stiffness. Specifically, to avoid ambiguities inherent in defining a local shear modulus, we utilize $k_B T / \langle u^2 \rangle$ for individual particles as a measure of “local stiffness” of the material. A comprehensive discussion of the quantification of these local elastic heterogeneity fluctuations can be found in the works of Zheng et al.^{112,113} Notably, nanoscale stiffness fluctuations have been directly observed in nanoprobe measurements on polymer films¹²⁰ and metallic glass materials,^{121,122} where the qualitative characteristics of these fluctuations closely resemble the results obtained from

color maps of local molecular stiffness. In recent works,^{22,51} we also discussed elastic fluctuations in linear and star polymers based on color maps of local molecular stiffness. It is then interesting to examine how knotting affects local molecular stiffness.

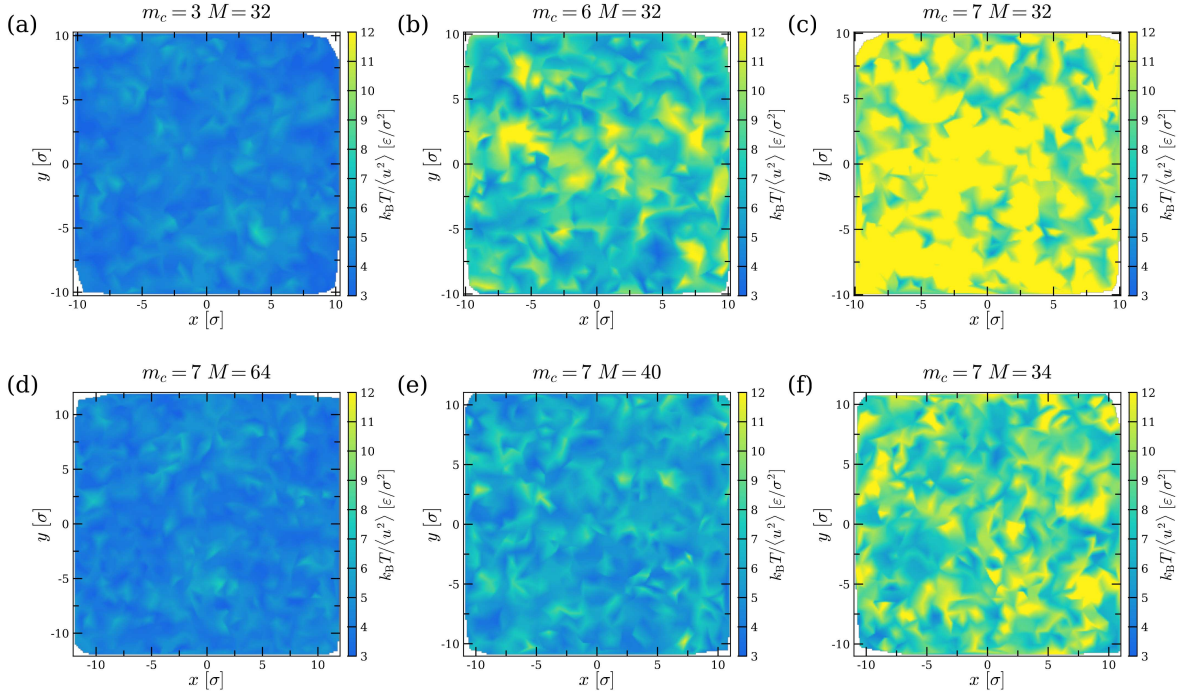


Figure 14: Color maps of local molecular stiffness $k_{\text{B}}T/\langle u^2 \rangle$. Panels (a–f) show the results for various combinations of m_c and M indicated in each panel at $T = 1.0\varepsilon/k_{\text{B}}$. For purposes of visualization, a slice with a thickness of 2σ is shown for each system.

Figure 14 presents color maps of local stiffness at $T = 1.0\varepsilon/k_{\text{B}}$ for various combinations of m_c and M . Within these maps, regions of relatively high local stiffness appear as yellow, while areas of lower stiffness are shown in blue. To enable direct comparisons in knotted ring polymer melts with varying parameters, a common colorbar scale is used for all systems. These maps reveal that both m_c and M substantially affect the spatial variation in local molecular stiffness. When m_c is relatively small at a fixed M , or when M is large at a fixed m_c , the color maps display predominantly uniform blue regions, suggesting a nearly homogeneous stiffness distribution at the specified T . Under the same thermodynamic conditions, the fluctuations in local stiffness grows progressively as m_c increases at a fixed M , and similarly as M increases at a fixed m_c . Specifically, increasing either m_c at a fixed M

or M at a fixed m_c enhances both the average stiffness and the range of fluctuations in the elastic heterogeneity of the polymer material. This occurs even as the packing efficiency of the molecules increases, resulting in a reduction of free volume as defined by density. This trend is quite reminiscent of the simulation observations on a model glass-forming polymer melt with an anti-plasticizing additive that reduces the fragility and increases the rigidity of the polymer composite material at low T .¹²³ Our previous study⁵⁰ demonstrated that fragility decreases with increasing m_c when M is small, and similarly, fragility decreases as M decreases for large m_c . Therefore, the observed increase in elastic heterogeneity with decreasing fragility is consistent with the established trends in glass-forming liquids.¹²³

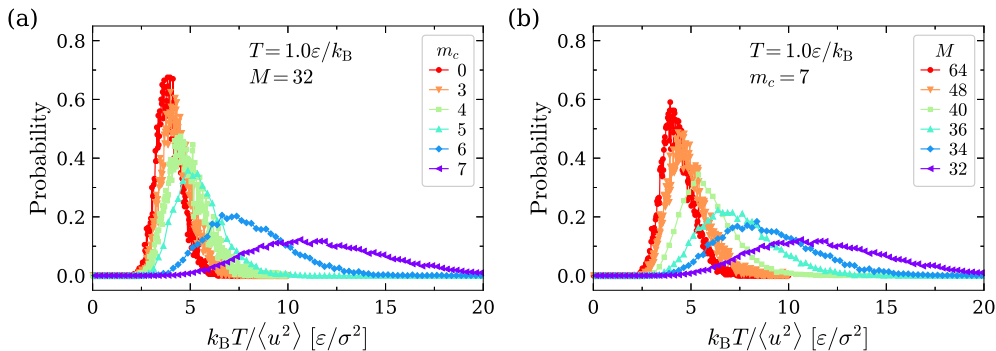


Figure 15: Probability distribution of local molecular stiffness $k_B T / \langle u^2 \rangle$. Panels (a) and (b) show the results for a range of m_c at $M = 32$ and for a range of M at $m_c = 7$ at $T = 1.0\epsilon/k_B$, respectively.

To further quantify the influence of knotting on local stiffness fluctuations, we analyze the probability distribution of local molecular stiffness, $k_B T / \langle u^2 \rangle$. Figure 15 shows the results for a range of m_c at fixed M and a range of M at fixed m_c at $T = 1.0\epsilon/k_B$. For small m_c or large M , it can be seen that a large amount of polymer segments exhibit a low local stiffness and that the shape of the distribution is characterized by a roughly single Gaussian peak, as in previous studies of stiffness fluctuations in simulated polymer materials.^{112,113} When m_c is larger than or equal to approximately 6, the average stiffness of the material, as inferred from $k_B T / \langle u^2 \rangle$, evidently becomes greatly enhanced, since the width of the peak grows progressively with increasing m_c and decreasing M . Notably, the probability distribution of local molecular stiffness has an additional peak in star polymers,⁵¹ reflecting the segments in

the star core regions, but this feature does not appear in knotted ring polymer melts. Overall, this analysis provides another example in which the reduction of fragility, associated with enhanced molecular packing and a reduced fragility of glass formation with higher knot complexity, leads to larger fluctuations in the local stiffness within the material.

Finally, we note that the observed abrupt changes in dynamic and elastic properties around $m_c \approx 5$ at low M can be understood through the lens of topological complexity and geometric constraints. Previous studies on knotted ring, star, and linear polymers have established an approximate correspondence where the properties of knotted rings track those of star polymers with $f \approx m_c + 5$ arms.¹²⁴ In star polymer melts, increasing f beyond approximately 5 causes a transition toward higher molecular symmetry, and the polymers begin to exhibit particle-like core-shell characteristics as f approaches a value on the order of 10. Our results indicate that a similar transition occurs in knotted ring melts, where high knot complexity induces a “particle-like” character and significantly increases structural rigidity. Crucially, unlike star polymers, knotted rings exhibit a progressive rigidification as their contour length approaches the minimal length required for a given knot topology to exist. In this “tight knot” limit, the segments become highly localized, and the structural relaxation time tends to diverge. Thus, the $m_c \approx 5$ threshold marks a crossover from random-coil-like behavior to a regime dominated by topological rigidification and a tendency to form particle-like structures, although the precise value of this threshold probably depends on chain stiffness and intermolecular interaction strength.

4 Summary

The enduring relevance of many models of glass formation developed over the years can be attributed to their success in rationalizing observations of real materials. In the present work, we extended our previous efforts to provide a more unified treatment of the dynamics of glass-forming liquids based on extensive simulation data of knotted ring polymer melts,

where cooperative motion, rigidity, and glassy dynamics can all be tuned over a wide range. Specifically, we demonstrated that the structural relaxation time can be quantitatively described by the string, localization, and shoving models, which emphasize cooperative particle motion, fluctuations in local particle mobility, and emergent elastic properties, respectively. A primary finding was that despite their superficially different formulations, these theoretical models of glass formation offer essentially equivalent descriptions of relaxation in knotted ring polymer melts. This observation suggested a promising potential for unification in the theories of glass-forming liquids. We also employed the non-Gaussian parameter to characterize dynamic heterogeneity and established the relationship between the peak time of the non-Gaussian parameter, the structural relaxation time, and the glassy plateau shear modulus. We also identified a new relation that links the peak time of the non-Gaussian parameter to the scale of collective motion, thereby connecting this dynamic heterogeneity parameter to the fragility of glass formation. Furthermore, we utilized color maps of local molecular stiffness to visualize the long-lived elastic heterogeneity of knotted ring polymer melts. Overall, our findings reveal a satisfying convergence among distinct theoretical frameworks based on a highly tunable model system. This convergence not only validates the core physical insights embedded in each model but also underscores that the essence of glassy dynamics may be captured by multiple, interrelated physical quantities.

Acknowledgement

W.-S.X. acknowledges the support from the National Natural Science Foundation of China (Nos. 22573102 and 22222307). This research used resources of the Network and Computing Center at Changchun Institute of Applied Chemistry, Chinese Academy of Sciences. The authors thank Dr. Fernando Vargas-Lara at ExxonMobil Technology and Engineering Company for sharing the initial knot configurations and helpful discussions about knotted rings. W.-S.X. and Y.-T.D. are grateful to Prof. Liang Dai at City University of

Hong Kong for useful discussions about knotted rings and for sharing the code for identifying knot types.

Supporting Information Available

Definition of basic dynamic properties, additional results about correlations between characteristic properties of glass formation, and influence of the caging onset time on model fits.

References

- (1) McKenna, G. B.; Simon, S. L. 50th Anniversary Perspective: Challenges in the Dynamics and Kinetics of Glass-Forming Polymers. *Macromolecules* **2017**, *50*, 6333–6361.
- (2) Debenedetti, P. G.; Stillinger, F. H. Supercooled Liquids and the Glass Transition. *Nature* **2001**, *410*, 259–267.
- (3) Berthier, L.; Biroli, G. Theoretical Perspective on the Glass Transition and Amorphous Materials. *Rev. Mod. Phys.* **2011**, *83*, 587–645.
- (4) Ediger, M. D.; Harrowell, P. Perspective: Supercooled Liquids and Glasses. *J. Chem. Phys.* **2012**, *137*, 080901.
- (5) Biroli, G.; Garrahan, J. P. Perspective: The Glass Transition. *J. Chem. Phys.* **2013**, *138*, 12A301.
- (6) Debenedetti, P. G.; Stillinger, F. H. Glass Transition Thermodynamics and Kinetics. *Annu. Rev. Condens. Matter Phys.* **2013**, *4*, 263–285.
- (7) Cohen, M. H.; Turnbull, D. Molecular Transport in Liquids and Glasses. *J. Chem. Phys.* **1959**, *31*, 1164–1169.

- (8) Turnbull, D.; Cohen, M. H. Free-Volume Model of the Amorphous Phase: Glass Transition. *J. Chem. Phys.* **1961**, *34*, 120–125.
- (9) Adam, G.; Gibbs, J. H. On the Temperature Dependence of Cooperative Relaxation Properties in Glass-Forming Liquids. *J. Chem. Phys.* **1965**, *43*, 139–146.
- (10) Götze, W. *Complex Dynamics of Glass-Forming Liquids: A Mode-Coupling Theory*; Oxford University Press, Oxford, 2008.
- (11) Leutheusser, E. Dynamical model of the liquid-glass transition. *Phys. Rev. A* **1984**, *29*, 2765–2773.
- (12) Fredrickson, G. H.; Andersen, H. C. Dynamics of supercooled liquids and the glass-transition. *J. Phys. C* **1984**, *17*, 5915–5934.
- (13) Mézard, M.; Parisi, G.; Virasoro, M. *Spin glass theory and beyond*; World Scientific, 1988.
- (14) Freed, K. F. Communication: Towards First Principles Theory of Relaxation in Supercooled Liquids Formulated in Terms of Cooperative Motion. *J. Chem. Phys.* **2014**, *141*, 141102.
- (15) Pazmiño Betancourt, B. A.; Douglas, J. F.; Starr, F. W. String Model for the Dynamics of Glass-Forming Liquids. *J. Chem. Phys.* **2014**, *140*, 204509.
- (16) Simmons, D. S.; Cicerone, M. T.; Zhong, Q.; Tyagi, M.; Douglas, J. F. Generalized Localization Model of Relaxation in Glass-Forming Liquids. *Soft Matter* **2012**, *8*, 11455–11461.
- (17) Douglas, J. F.; Pazmino Betancourt, B. A.; Tong, X.; Zhang, H. Localization Model Description of Diffusion and Structural Relaxation in Glass-Forming Cu–Zr Alloys. *J. Stat. Mech.: Theory Exp.* **2016**, *2016*, 054048.

- (18) Dyre, J. C. Colloquium: The Glass Transition and Elastic Models of Glass-Forming Liquids. *Rev. Mod. Phys.* **2006**, *78*, 953–972.
- (19) Dyre, J. C.; Wang, W. H. The Instantaneous Shear Modulus in the Shoving Model. *J. Chem. Phys.* **2012**, *136*, 224108.
- (20) Hecksher, T.; Dyre, J. C. A Review of Experiments Testing the Shoving Model. *J. Non-Cryst. Solids* **2015**, *407*, 14–22.
- (21) Pazmiño Betancourt, B. A.; Hanakata, P. Z.; Starr, F. W.; Douglas, J. F. Quantitative Relations between Cooperative Motion, Emergent Elasticity, and Free Volume in Model Glass-Forming Polymer Materials. *Proc. Natl. Acad. Sci. U. S. A.* **2015**, *112*, 2966–2971.
- (22) Xu, X.; Douglas, J. F.; Xu, W.-S. Parallel Emergence of Rigidity and Collective Motion in a Family of Simulated Glass-Forming Polymer Fluids. *Macromolecules* **2023**, *56*, 4929–4951.
- (23) Yuan, Q.-L.; Xu, X.; Xu, W.-S.; Douglas, J. F. Understanding Relaxation in the Kob-Andersen Liquid Based on Entropy, String, Shoving, Localization, and Parabolic Models. *J. Phys. Chem. B* **2024**, *128*, 10999–11021.
- (24) Dudowicz, J.; Freed, K. F.; Douglas, J. F. Generalized entropy theory of polymer glass formation. *Adv. Chem. Phys.* **2008**, *137*, 125–222.
- (25) Xu, W.-S.; Douglas, J. F.; Sun, Z.-Y. Polymer Glass Formation: Role of Activation Free Energy, Configurational Entropy, and Collective Motion. *Macromolecules* **2021**, *54*, 3001–3033.
- (26) Xu, W.-S.; Sun, Z.-Y. A Thermodynamic Perspective on Polymer Glass Formation. *Chinese J. Polym. Sci.* **2023**, *41*, 1329–1341.

- (27) Yuan, Q.-L.; Yang, Z.; Xu, W.-S. Advances in the Generalized Entropy Theory of Polymer Glass Formation. *Sci. Sin. Chim.* **2023**, *53*, 616–627.
- (28) Foreman, K. W.; Freed, K. F. Lattice Cluster Theory of Multicomponent Polymer Systems: Chain Semiflexibility and Specific Interactions. *Adv. Chem. Phys.* **1998**, 335–390.
- (29) Xu, W.-S.; Freed, K. F. Lattice Cluster Theory for Polymer Melts with Specific Interactions. *J. Chem. Phys.* **2014**, *141*, 044909.
- (30) Xu, X.; Douglas, J. F.; Xu, W.-S. Thermodynamic–Dynamic Interrelations in Glass-Forming Polymer Fluids. *Macromolecules* **2022**, *55*, 8699–8722.
- (31) Caruthers, J. M.; Medvedev, G. A. Quantitative Model of Super-Arrhenian Behavior in Glass Forming Materials. *Phys. Rev. Materials* **2018**, *2*, 055604.
- (32) Medvedev, G. A.; Caruthers, J. M. A Quantitative Model of Super-Arrhenian Behavior in Glass-Forming Polymers. *Macromolecules* **2019**, *52*, 1424–1439.
- (33) Zhao, X.; Simon, S. L. A Model-Free Analysis of Configurational Properties to Reduce the Temperature- and Pressure-Dependent Segmental Relaxation Times of Polymers. *J. Chem. Phys.* **2020**, *152*, 044901.
- (34) Rybenkov, V. V.; Cozzarelli, N. R.; Vologodskii, A. V. Probability of DNA knotting and the effective diameter of the DNA double helix. *Proc. Natl. Acad. Sci. U. S. A.* **1993**, *90*, 5307–5311.
- (35) Shaw, S. Y.; Wang, J. C. Knotting of a DNA chain during ring closure. *Science* **1993**, *260*, 533–536.
- (36) Ercolini, E.; Valle, F.; Adamcik, J.; Witz, G.; Metzler, R.; De Los Rios, P.; Roca, J.; Dietler, G. Fractal Dimension and Localization of DNA Knots. *Phys. Rev. Lett.* **2007**, *98*, 058102.

- (37) Taylor, W. R. A deeply knotted protein structure and how it might fold. *Nature* **2000**, *406*, 916–919.
- (38) Jamroz, M.; Niemyska, W.; Rawdon, E. J.; Stasiak, A.; Millett, K. C.; Sułkowski, P.; Sulkowska, J. I. KnotProt: a database of proteins with knots and slipknots. *Nucleic Acids Res.* **2015**, *43*, D306–D314.
- (39) Bornschlögl, T.; Anstrom, D. M.; Mey, E.; Dzubiella, J.; Rief, M.; Forest, K. T. Tightening the Knot in Phytochrome by Single-Molecule Atomic Force Microscopy. *Biophys. J.* **2009**, *96*, 1508–1514.
- (40) Virnau, P.; Kantor, Y.; Kardar, M. Knots in Globule and Coil Phases of a Model Polyethylene. *J. Am. Chem. Soc.* **2005**, *127*, 15102–15106.
- (41) Majumder, S.; Marenz, M.; Paul, S.; Janke, W. Knots are Generic Stable Phases in Semiflexible Polymers. *Macromolecules* **2021**, *54*, 5321–5334.
- (42) Wu, Z.; Alberti, S. A. N.; Schneider, J.; Müller-Plathe, F. Knotting behaviour of polymer chains in the melt state for soft-core models with and without slip-springs. *J. Phys.: Condens. Matter* **2021**, *33*, 244001.
- (43) Saitta, A. M.; Soper, P. D.; Wasserman, E.; Klein, M. L. Influence of a Knot on the Strength of a Polymer Strand. *Nature* **1999**, *399*, 46–48.
- (44) Tang, J.; Du, N.; Doyle, P. S. Compression and self-entanglement of single DNA molecules under uniform electric field. *Proc. Natl. Acad. Sci. U.S.A.* **2011**, *108*, 16153–16158.
- (45) Huang, L.; Makarov, D. E. Translocation of a knotted polypeptide through a pore. *J. Chem. Phys.* **2008**, *129*, 121107.

- (46) Rosa, A.; Di Ventra, M.; Micheletti, C. Topological Jamming of Spontaneously Knotted Polyelectrolyte Chains Driven Through a Nanopore. *Phys. Rev. Lett.* **2012**, *109*, 118301.
- (47) Renner, C. B.; Doyle, P. S. Stretching self-entangled DNA molecules in elongational fields. *Soft Matter* **2015**, *11*, 3105–3114.
- (48) Klotz, A. R.; Narsimhan, V.; Soh, B. W.; Doyle, P. S. Dynamics of DNA Knots during Chain Relaxation. *Macromolecules* **2017**, *50*, 4074–4082.
- (49) Meluzzi, D.; Smith, D. E.; Arya, G. Biophysics of Knotting. *Annu. Rev. Biophys.* **2010**, *39*, 349–366.
- (50) Dong, Y.-T.; Song, X.-Y.; Xu, X.; Jiang, S.; Douglas, J. F.; Sun, Z.-Y.; Xu, W.-S. Glass Formation in Ring Polymer Melts Having Variable Knot Complexity and Molecular Mass. *Macromolecules* **2024**, *57*, 6875–6896.
- (51) Yang, Z.; Xu, X.; Douglas, J. F.; Xu, W.-S. Confinement Effect of Inter-Arm Interactions on Glass Formation in Star Polymer Melts. *J. Chem. Phys.* **2024**, *160*, 044503.
- (52) Kob, W.; Andersen, H. C. Testing mode-coupling theory for a supercooled binary Lennard-Jones mixture I: The van Hove correlation function. *Phys. Rev. E* **1995**, *51*, 4626–4641.
- (53) Kob, W.; Andersen, H. C. Testing mode-coupling theory for a supercooled binary Lennard-Jones mixture. II. Intermediate scattering function and dynamic susceptibility. *Phys. Rev. E* **1995**, *52*, 4134–4153.
- (54) Ashbridge, Z.; Fielden, S. D. P.; Leigh, D. A.; Pirvu, L.; Schaufelberger, F.; Zhang, L. Knotting matters: orderly molecular entanglements. *Chem. Soc. Rev.* **2022**, *51*, 7779–7809.

- (55) Wang, W. et al. What Can Topology Bring to Chemistry? *CCS Chem.* **2024**, *6*, 2084–2109.
- (56) Cunha, L. H. P.; Tubiana, L.; Biswal, S. L.; MacKintosh, F. C. Hierarchical Knot Formation of Semiflexible Filaments Driven by Hydrodynamics. *Phys. Rev. Lett.* **2025**, *135*, 248201.
- (57) Marcos, V.; Stephens, A. J.; Jaramillo-Garcia, J.; Nussbaumer, A. L.; Woltering, S. L.; Valero, A.; Lemonnier, J.-F.; Vitorica-Yrezabal, I. J.; Leigh, D. A. Allosteric initiation and regulation of catalysis with a molecular knot. *Science* **2016**, *352*, 1555–1559.
- (58) Christian, T.; Sakaguchi, R.; Perlinska, A. P.; Lahoud, G.; Ito, T.; Taylor, E. A.; Yokoyama, S.; Sulkowska, J. I.; Hou, Y.-M. Methyl transfer by substrate signaling from a knotted protein fold. *Nat. Struct. Mol. Biol.* **2016**, *23*, 941–948.
- (59) Hsu, S.-T. D. Folding and functions of knotted proteins. *Curr. Opin. Struct. Biol.* **2023**, *83*, 102709.
- (60) Kremer, K.; Grest, G. S. Dynamics of Entangled Linear Polymer Melts: A Molecular-Dynamics Simulation. *J. Chem. Phys.* **1990**, *92*, 5057–5086.
- (61) Grest, G. S.; Kremer, K. Molecular Dynamics Simulation for Polymers in the Presence of a Heat Bath. *Phys. Rev. A* **1986**, *33*, 3628–3631.
- (62) Vargas-Lara, F.; Betancourt, B. A. P.; Douglas, J. F. Influence of Knot Complexity on Glass-Formation in Low Molecular Mass Ring Polymer Melts. *J. Chem. Phys.* **2019**, *150*, 101103.
- (63) Inc., W. R. Mathematica, Version 12.3. Champaign, IL, 2021.
- (64) Thompson, A. P.; Aktulga, H. M.; Berger, R.; Bolintineanu, D. S.; Brown, W. M.; Crozier, P. S.; in 't Veld, P. J.; Kohlmeyer, A.; Moore, S. G.; Nguyen, T. D.; Shan, R.;

- Stevens, M. J.; Tranchida, J.; Trott, C.; Plimpton, S. J. LAMMPS - a flexible simulation tool for particle-based materials modeling at the atomic, meso, and continuum scales. *Comp. Phys. Comm.* **2022**, *271*, 108171.
- (65) Lammmps version: June 23, 2022. Retrieved from <http://lammmps.sandia.gov>.
- (66) Qiu, Q.-Y.; Zhu, Y.-J.; Wu, Z.-T.; Dai, L. A Simple and Efficient Algorithm to Identify the Chirality of Polymer Knots Based on the Alexander Polynomial. *Chinese J. Polym. Sci.* **2024**, *42*, 2030–2037.
- (67) Song, X.-Y.; Yang, Z.-Y.; Yuan, Q.-L.; Li, S.-W.; Tang, Z.-Q.; Dong, Y.-T.; Jiang, S.-C.; Xu, W.-S. Understanding Mass Dependence of Glass Formation in Ring Polymers. *Chinese J. Polym. Sci.* **2023**, *41*, 1447–1461.
- (68) Donati, C.; Douglas, J. F.; Kob, W.; Plimpton, S. J.; Poole, P. H.; Glotzer, S. C. Stringlike Cooperative Motion in a Supercooled Liquid. *Phys. Rev. Lett.* **1998**, *80*, 2338–2341.
- (69) Aichele, M.; Gebremichael, Y.; Starr, F. W.; Baschnagel, J.; Glotzer, S. C. Polymer-Specific Effects of Bulk Relaxation and Stringlike Correlated Motion in the Dynamics of a Supercooled Polymer Melt. *J. Chem. Phys.* **2003**, *119*, 5290–5304.
- (70) Starr, F. W.; Douglas, J. F. Modifying Fragility and Collective Motion in Polymer Melts with Nanoparticles. *Phys. Rev. Lett.* **2011**, *106*, 115702.
- (71) Pazmiño Betancourt, B. A.; Douglas, J. F.; Starr, F. W. Fragility and Cooperative Motion in a Glass-Forming Polymer-Nanoparticle Composite. *Soft Matter* **2013**, *9*, 241–254.
- (72) Starr, F. W.; Douglas, J. F.; Sastry, S. The Relationship of Dynamical Heterogeneity to the Adam-Gibbs and Random First-Order Transition Theories of Glass Formation. *J. Chem. Phys.* **2013**, *138*, 12A541.

- (73) Hanakata, P. Z.; Douglas, J. F.; Starr, F. W. Interfacial Mobility Scale Determines the Scale of Collective Motion and Relaxation Rate in Polymer Films. *Nat. Commun.* **2014**, *5*, 4163.
- (74) Hanakata, P. Z.; Pazmiño Betancourt, B. A.; Douglas, J. F.; Starr, F. W. A Unifying Framework to Quantify the Effects of Substrate Interactions, Stiffness, and Roughness on the Dynamics of Thin Supported Polymer Films. *J. Chem. Phys.* **2015**, *142*, 234907.
- (75) Xu, W.-S.; Douglas, J. F.; Freed, K. F. Influence of Cohesive Energy on Relaxation in a Model Glass-Forming Polymer Melt. *Macromolecules* **2016**, *49*, 8355–8370.
- (76) Xu, W.-S.; Douglas, J. F.; Freed, K. F. Stringlike Cooperative Motion Explains the Influence of Pressure on Relaxation in a Model Glass-Forming Polymer Melt. *ACS Macro Lett.* **2016**, *5*, 1375–1380.
- (77) Xu, W.-S.; Douglas, J. F.; Freed, K. F. Influence of Pressure on Glass Formation in a Simulated Polymer Melt. *Macromolecules* **2017**, *50*, 2585–2598.
- (78) Zhang, W.; Starr, F. W.; Douglas, J. F. Collective Motion in the Interfacial and Interior Regions of Supported Polymer Films and Its Relation to Relaxation. *J. Phys. Chem. B* **2019**, *123*, 5935–5941.
- (79) Fan, J.; Emamy, H.; Chremos, A.; Douglas, J. F.; Starr, F. W. Dynamic Heterogeneity and Collective Motion in Star Polymer Melts. *J. Chem. Phys.* **2020**, *152*, 054904.
- (80) Zhang, H.; Zhong, C.; Douglas, J. F.; Wang, X.; Cao, Q.; Zhang, D.; Jiang, J.-Z. Role of String-like Collective Atomic Motion on Diffusion and Structural Relaxation in Glass Forming Cu-Zr Alloys. *J. Chem. Phys.* **2015**, *142*, 164506.
- (81) Kincaid, J. F.; Eyring, H.; Stearn, A. E. The Theory of Absolute Reaction Rates and

- Its Application to Viscosity and Diffusion in the Liquid State. *Chem. Rev.* **1941**, *28*, 301–365.
- (82) Glasstone, S.; Laidler, K. J.; Eyring, H. *The Theory of Rate Processes: The Kinetics of Chemical Reactions, Viscosity, Diffusion and Electrochemical Phenomena*; International Chemical Series; McGraw-Hill Book Company: Incorporated, 1941.
- (83) Jeong, C.; Douglas, J. F. Mass Dependence of the Activation Enthalpy and Entropy of Unentangled Linear Alkane Chains. *J. Chem. Phys.* **2015**, *143*, 144905.
- (84) Gelin, S.; Champagne-Ruel, A.; Mousseau, N. Enthalpy-Entropy Compensation of Atomic Diffusion Originates from Softening of Low Frequency Phonons. *Nat. Commun.* **2020**, *11*, 3977.
- (85) Xu, W.-S.; Douglas, J. F.; Xu, X. Role of Cohesive Energy in Glass Formation of Polymers with and without Bending Constraints. *Macromolecules* **2020**, *53*, 9678–9697.
- (86) Xu, W.-S.; Douglas, J. F.; Xia, W.; Xu, X. Investigation of the Temperature Dependence of Activation Volume in Glass-Forming Polymer Melts under Variable Pressure Conditions. *Macromolecules* **2020**, *53*, 6828–6841.
- (87) Xu, W.-S.; Douglas, J. F.; Xu, X. Molecular Dynamics Study of Glass Formation in Polymer Melts with Varying Chain Stiffness. *Macromolecules* **2020**, *53*, 4796–4809.
- (88) Larini, L.; Ottochian, A.; De Michele, C.; Leporini, D. Universal Scaling between Structural Relaxation and Vibrational Dynamics in Glass-Forming Liquids and Polymers. *Nature Phys.* **2008**, *4*, 42–45.
- (89) Ottochian, A.; De Michele, C.; Leporini, D. Universal Divergenceless Scaling between Structural Relaxation and Caged Dynamics in Glass-Forming Systems. *J. Chem. Phys.* **2009**, *131*, 224517.

- (90) Ottochian, A.; Leporini, D. Universal Scaling between Structural Relaxation and Caged Dynamics in Glass-Forming Systems: Free Volume and Time Scales. *J. Non-Cryst. Solids* **2011**, *357*, 298–301.
- (91) Puosi, F.; Leporini, D. Scaling between Relaxation, Transport, and Caged Dynamics in Polymers: From Cage Restructuring to Diffusion. *J. Phys. Chem. B* **2011**, *115*, 14046–14051.
- (92) Starr, F. W.; Sastry, S.; Douglas, J. F.; Glotzer, S. C. What Do We Learn from the Local Geometry of Glass-Forming Liquids? *Phys. Rev. Lett.* **2002**, *89*, 125501.
- (93) Wang, X.; Zhang, H.; Douglas, J. F. The Initiation of Shear Band Formation in Deformed Metallic Glasses from Soft Localized Domains. *J. Chem. Phys.* **2021**, *155*, 204504.
- (94) McKenzie-Smith, T. Q.; Douglas, J. F.; Starr, F. W. Explaining the Sensitivity of Polymer Segmental Relaxation to Additive Size Based on the Localization Model. *Phys. Rev. Lett.* **2021**, *127*, 277802.
- (95) McKenzie-Smith, T.; Douglas, J. F.; Starr, F. W. Relating dynamic free volume to cooperative relaxation in a glass-forming polymer composite. *J. Chem. Phys.* **2022**, *157*, 131101.
- (96) Mahmud, G.; Zhang, H.; Douglas, J. Localization Model Description of the Interfacial Dynamics of Crystalline Cu and $Cu_{64}Zr_{36}$ Metallic Glass Nanoparticles. *Eur. Phys. J. E* **2021**, *44*, 33.
- (97) Mahmud, G.; Zhang, H.; Douglas, J. F. The dynamics of metal nanoparticles on a supporting interacting substrate. *J. Chem. Phys.* **2022**, *157*, 114505.
- (98) Mangalara, J. H.; Simmons, D. S. Tuning polymer glass formation behavior and me-

- chanical properties with oligomeric diluents of varying stiffness. *ACS Macro Lett.* **2015**, *4*, 1134–1138.
- (99) Ruan, D.; Simmons, D. S. Roles of chain stiffness and segmental rattling in ionomer glass formation. *J. Polym. Sci., Part B: Polym. Phys.* **2015**, *53*, 1458–1469.
- (100) Douglas, J. F.; Yuan, Q.-L.; Zhang, J.; Zhang, H.; Xu, W.-S. A dynamical system approach to relaxation in glass-forming liquids. *Soft Matter* **2024**, *20*, 9140–9160.
- (101) Pazmiño Betancourt, B. A.; Starr, F. W.; Douglas, J. F. String-like Collective Motion in the α - and β -Relaxation of a Coarse-Grained Polymer Melt. *J. Chem. Phys.* **2018**, *148*, 104508.
- (102) Yuan, Q.-L.; Xu, X.; Douglas, J. F.; Xu, W.-S. Influence of Density and Pressure on Glass Formation in the Kob-Andersen Model. *J. Phys. Chem. B* **2024**, *128*, 9889–9904.
- (103) Ngai, K. L.; Bao, L.-R.; Yee, A. F.; Soles, C. L. Correlation of Positron Annihilation and Other Dynamic Properties in Small Molecule Glass-Forming Substances. *Phys. Rev. Lett.* **2001**, *87*, 215901.
- (104) Bastow, T. J.; Mair, S. L.; Wilkins, S. W. Empirical $T^{3/2}$ law for atomic thermal vibration parameters. *J. Appl. Phys.* **1977**, *48*, 494–497.
- (105) Marcus, M.; Tsai, C.-L. EXAFS measurements of lattice vibrations of Ti and Cu in Ti. *Solid State Commun.* **1984**, *52*, 511–513.
- (106) Van Hung, N.; Rehr, J. Anharmonic correlated Einstein-model Debye-Waller factors. *Phys. Rev. B* **1997**, *56*, 43.
- (107) Puosi, F.; Leporini, D. Communication: Correlation of the Instantaneous and the Intermediate-Time Elasticity with the Structural Relaxation in Glassforming Systems. *J. Chem. Phys.* **2012**, *136*, 041104.

- (108) Kojima, S.; Sato, H.; Yosihara, A. Light Scattering of Supercooled Propylene Glycol. *J. Phys.: Condens. Matter* **1997**, *9*, 10079.
- (109) Novikov, V. Fast Relaxation in Glasses: Relation to Free Volume and Anharmonicity. *Prog. Theor. Phys. Suppl.* **1997**, *126*, 159–162.
- (110) Giuntoli, A.; Puosi, F.; Leporini, D.; Starr, F. W.; Douglas, J. F. Predictive Relation for the α -Relaxation Time of a Coarse-Grained Polymer Melt under Steady Shear. *Sci. Adv.* **2020**, *6*, eaaz0777.
- (111) Puosi, F.; Leporini, D. The Kinetic Fragility of Liquids as Manifestation of the Elastic Softening. *Eur. Phys. J. E* **2015**, *38*, 87.
- (112) Zheng, X.; Guo, Y.; Douglas, J. F.; Xia, W. Understanding the Role of Cross-Link Density in the Segmental Dynamics and Elastic Properties of Cross-Linked Thermosets. *J. Chem. Phys.* **2022**, *157*, 064901.
- (113) Zheng, X.; Guo, Y.; Douglas, J. F.; Xia, W. Competing Effects of Cohesive Energy and Cross-Link Density on the Segmental Dynamics and Mechanical Properties of Cross-Linked Polymers. *Macromolecules* **2022**, *55*, 9990–10004.
- (114) Douglas, J. F.; Xu, W.-S. Equation of State and Entropy Theory Approach to Thermodynamic Scaling in Polymeric Glass-Forming Liquids. *Macromolecules* **2021**, *54*, 3247–3269.
- (115) Jeong, C.; Starr, F. W.; Beers, K. L.; Douglas, J. F. Influence of Functionalization on the Crystallinity and Basic Thermodynamic Properties of Polyethylene. *Macromolecules* **2023**, *56*, 3873–3883.
- (116) Zheng, X.; Nie, W.; Guo, Y.; Douglas, J. F.; Xia, W. Influence of Chain Stiffness on the Segmental Dynamics and Mechanical Properties of Cross-Linked Polymers. *Macromolecules* **2023**, *56*, 7636–7650.

- (117) Zhang, W.; Starr, F. W.; Douglas, J. F. Activation Free Energy Gradient Controls Interfacial Mobility Gradient in Thin Polymer Films. *J. Chem. Phys.* **2021**, *155*, 174901.
- (118) de Gennes, P. G. Tight knots. *Macromolecules* **1984**, *17*, 703–704.
- (119) Xu, X.; Douglas, J. F.; Xu, W.-S. Generalized entropy theory investigation of the relatively high segmental fragility of many glass-forming polymers. *Soft Matter* **2025**, *21*, 2664–2685.
- (120) Nguyen, H. K.; Wang, D.; Russell, T. P.; Nakajima, K. Observation of Dynamical Heterogeneities and Their Time Evolution on the Surface of an Amorphous Polymer. *Soft Matter* **2015**, *11*, 1425–1433.
- (121) Liu, Y. H.; Wang, D.; Nakajima, K.; Zhang, W.; Hirata, A. Characterization of Nanoscale Mechanical Heterogeneity in a Metallic Glass by Dynamic Force Microscopy. *Phys. Rev. Lett.* **2011**, *106*, 125504.
- (122) Wang, D. P.; Qiao, J. C.; Liu, C. T. Relating Structural Heterogeneity to β Relaxation Processes in Metallic Glasses. *Mater. Res. Lett.* **2019**, *7*, 305–311.
- (123) Riggleman, R. A.; Douglas, J. F.; De Pablo, J. J. Antiplasticization and the Elastic Properties of Glass-Forming Polymer Liquids. *Soft Matter* **2010**, *6*, 292–304.
- (124) Vargas-Lara, F.; Pazmiño Betancourt, B. A.; Douglas, J. F. Communication: A Comparison between the Solution Properties of Knotted Ring and Star Polymers. *J. Chem. Phys.* **2018**, *149*, 161101.

TOC Graphic

